Geophys. J. Int. (2004) **158,** 1134–1150 doi: 10.1111/j.1365-246X.2004.02312.x

The effects of buoyant crust on the gravitational instability of thickened mantle lithosphere at zones of intracontinental convergence

Peter Molnar[1] and Gregory A. Houseman[2]

[1]*Department of Geological Sciences and Cooperative Institute for Research in Environmental Science (CIRES), University of Colorado at Boulder, Boulder, CO* 80309-0399, *USA*
[2]*School of Earth Sciences, University of Leeds, Leeds* LS2 9JT, *UK*

Accepted 2004 March 5. Received 2004 March 5; in original form 2003 March 19

SUMMARY

Using both numerical experiments and approximate linear theory, we examine the stability of a 2-D, three-layered viscous system that represents crust over mantle lithosphere, overlying asthenosphere. If horizontal shortening of lithosphere occurs, as in mountain building, the development of gravitational instability may follow one of two distinct paths. Localized downwelling occurs beneath the region of horizontal shortening and crustal thickening, if the layer representing crust has a large viscosity coefficient, is relatively dense or is thin, relative to the underlying layer that represents mantle lithosphere. Conversely, for a low viscosity ratio or buoyant crust, downwelling flow develops on the flanks of the zone of convergence, and the mantle lithosphere layer thins beneath the central region. Thinning in such a setting would facilitate volcanism and high-temperature metamorphism during the development of a mountain belt. A series of numerical experiments with different density and viscosity structures, including runs with non-Newtonian viscosity, show that this general description is insensitive to minor differences in the depth distributions of density and viscosity. The tendency of structures with relatively thick crustal layers (or relatively thin lithospheric mantle) to favour paired, marginal downwellings may account for sustained volcanism during intracontinental deformation where lithosphere initially is warm, thin and weak. The western part of the Tien Shan in Asia and the region including and surrounding the Alboran Sea illustrate some of the features associated with paired, marginal downwellings. The Western Transverse Ranges of California and the Southern Alps of New Zealand share features associated with single downwelling flow beneath the axes of the belts.

Key words: geodynamics, intracontinental tectonics, Rayleigh–Taylor instability.

INTRODUCTION

Where continental lithosphere shortens horizontally and crust thickens to build a mountain belt, mantle lithosphere must also shorten. In the simplest model of this process, mantle lithosphere thickens by pure shear beneath the thickening crust. If it is negatively buoyant, thickening lithosphere becomes increasingly unstable. Gravity pulls the excess thickness of relatively dense mantle lithosphere downward, creating the potential for rapid convective flow and removal of at least part of the mantle lithosphere underlying the thickened crust (Houseman *et al.* 1981). Although the relevance of this idealized process to actual orogenic events remains controversial, it provides an explanation for a number of phenomena that have been widely observed in the latter stages of mountain building. Not only Barrovian (regional) metamorphism, but also magmatic intrusions, and in some cases volcanism, occur during the development of mountain ranges (e.g. Miyashiro 1973; Sengör & Kidd 1979; McKenna & Walker 1990; Pearce *et al.* 1990; Kay & Mahlburg Kay 1993). If mantle lithosphere is removed during orogenesis, late orogenic or post-orogenic magmatic processes could owe their occurrence to thinning of the mantle lithosphere and the approach of a steepened temperature gradient to the solidus, such that mantle lithosphere and crust melt (e.g. Houseman *et al.* 1981; Arnaud *et al.* 1992; Turner *et al.* 1993, 1996, 1999). Decompression melting within the asthenosphere rising to sufficiently shallow depths might also occur. Without convective thinning of the lithosphere, the thickening caused by convergence should depress isotherms, and the diffusive transport of heat would require that reheating of the lithosphere would occur only slowly (England & Thompson 1984) compared with the timescales involved in both mountain building and erosion. Convective removal of mantle lithosphere, however, allows relatively rapid heating of both crust and mantle lithosphere after thickening has occurred. Moreover, the convective removal may trigger horizontal extension of both layers (England & Houseman 1989).

We start from the assumption that straining of the subcontinental mantle lithosphere is distributed broadly over a relatively

homogeneous layer (a width of ∼100–300 km), rather than being focused in narrow shear zones or suture zones (width of kilometres). In some circumstances this assumption is controversial, if not unrealistic, such as where continents have collided: the Alps or Himalaya. Mattauer (1986) suggested that lithosphere on one side of an intracontinental mountain belt coherently underthrusts the opposing plate, as at a collision zone. In this view the mantle lithosphere of the continents could be effectively subducted (e.g. Wellman 1979; Willett & Beaumont 1994), or delaminated (Bird 1978, 1979), beneath the deforming crustal layer. Others have suggested that the plate-like nature of the subcontinental mantle lithosphere is also evident in regions dominated by strike-slip deformation (e.g. Tapponnier *et al.* 1986, 2001). Plate-like deformation may be relevant in some circumstances, but we contend that there is also clear and specific evidence that distributed deformation dominates in other regions (e.g. England & Molnar 1997; Billen & Houseman 2004). There is a clear need to explore quantitatively the consequences of both views, though here we focus only on the latter.

We have carried out a number of studies aimed at determining the conditions under which thickened mantle lithosphere might become unstable and sink rapidly into the asthenosphere (Houseman *et al.* 1981, 2000; Conrad & Molnar 1997, 1999; Conrad 2000; Houseman & Molnar 1997, 2001; Molnar *et al.* 1998; Neil & Houseman 1999). These studies have been directed mainly toward determining the factors that affect the rate at which mantle lithosphere would be removed, and the fraction of it that should be removed in reasonable intervals of geological time. The connections between crustal thickening and the extent, timing and spatial relation of thinning of the mantle lithosphere, however, remain unclear. Previously it has been assumed that if convergence were restricted to a spatial domain comparable in width to the thickness of the lithosphere, downward flow of the mantle lithosphere would develop directly beneath the region of crustal thickening. Houseman *et al.* (2000), however, discovered a distinct mechanism by which rapid thinning of the mantle lithosphere can occur beneath the centre of the convergent zone, synchronous with forced localized convergence of the crustal layer. We pursue this mechanism further.

Houseman *et al.* (2000) considered a three-layered viscous fluid system, in which homogeneous layers representing respectively crust, mantle lithosphere and asthenosphere, undergo forced convergence in 2-D plane strain. They showed that the inclusion of a buoyant upper layer (crust) can profoundly affect the flow pattern in the underlying, negatively buoyant layer (mantle lithosphere). They examined the form of the instability that developed in the mantle lithosphere layer as it sinks into an inviscid substratum (asthenosphere). (In further discussion, we will refer to the three layers using these labels, making a distinction between the model layers and those in Earth only where their usage might be ambiguous.) Houseman *et al.* (2000) found that, depending largely on the ratio of viscosity of crust to that of mantle lithosphere, and weakly on the convergence rate (relative to the natural rate of development of gravitational instability), either a single downwelling sheet sank beneath the region of thickest crust (Figs 1a and d) or two downwelling sheets descended beneath its flanks (Figs 1c and e). Moreover, as can be seen in Fig. 1, in general when paired marginal downwellings flank the convergent zone, the mantle lithosphere beneath the centre of the zone thins.

We examine further the conditions under which such thinning of mantle lithosphere can occur. We consider lithospheric structures that are initially stratified (both homogeneous and depth dependent) and show that density, thickness and viscosity all affect the pattern of downwelling beneath the thickening crust. To gain some understanding of the mechanical process, we extend Neil & Houseman's (1999) analysis of linear stability by including the effect of externally forced thickening in an approximate way. In a final series of experiments we also consider non-Newtonian viscosity.

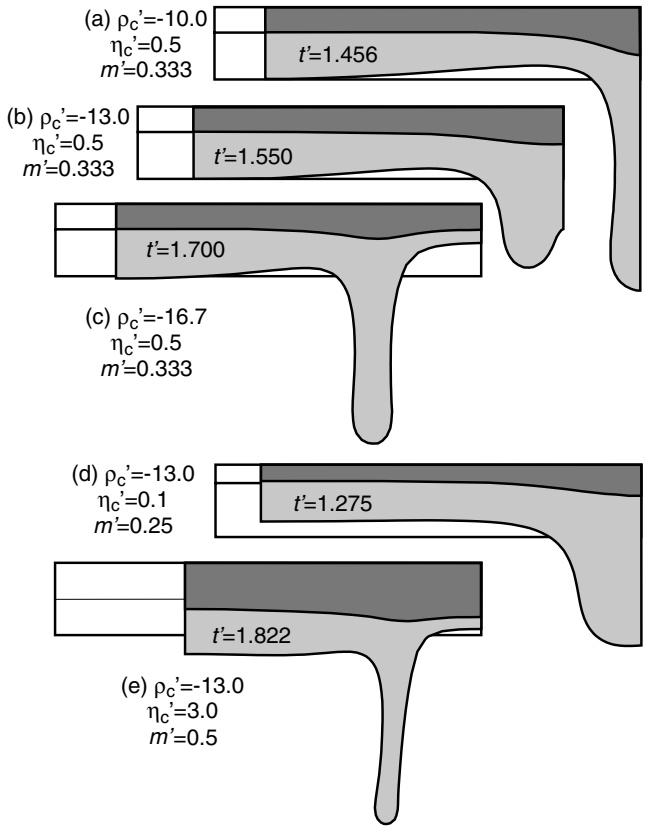

Figure 1. Cross-sections showing the shape of crustal (dark grey) and mantle lithospheric (light grey) layers after elapsed dimensionless times t' as shown, for five runs with forced convergence with different combinations of the key parameters, ρ_c', η_c' and m', all with $U_0' = 0.04$. Only the left half of the symmetric calculation is shown, with the plane of reflection symmetry on the right-hand side in each case. The white rectangles in the background show the pre-deformation shapes.

BASIC MODEL AND GOVERNING EQUATIONS

Much of the work referred to above, including that of Houseman *et al.* (2000), considered Rayleigh–Taylor instability, the instability that results from a dense layer overlying a less dense layer in a gravity field. The basic governing equations are those of Stokes flow, with the stress balance represented by

$$\frac{\partial \sigma_{ij}}{\partial x_j} - \rho g \delta_{iz} = 0. \quad (1)$$

As listed in Table 1, σ_{ij} are the stress components, x_j are the spatial coordinates, ρ is density, g is gravity and δ_{iz} is the Kronecker delta. Stress consists of isotropic (p) and deviatoric (τ_{ij}) parts:

$$\sigma_{ij} = p\delta_{ij} + \tau_{ij}. \quad (2)$$

We write the constitutive relations between deviatoric stress and strain rate as:

$$\tau_{ij} = BE^{(1-n)/n} e_{ij}. \quad (3)$$

Table 1. List of symbols.

a	Subscript referring to asthenosphere
c	Subscript referring to crust
g	Gravitational acceleration
l	Subscript referring to mantle lithosphere
m	Crustal thickness
n	Exponent in constitutive relationship between stress and strain rate
t	Time
x	Horizontal coordinate
z	Vertical coordinate
B	Viscosity coefficient for non-Newtonian viscosity
L	Thickness of lithosphere
U_0	Horizontal component of velocity applied to the lithosphere
η	Newtonian viscosity
ρ	Density
$\Delta\rho$	Difference in density between mantle lithosphere and asthenosphere
σ_{ij}	Components of stress

Here B is a viscosity coefficient, E is the second invariant of the strain-rate tensor, e_{ij}, and n describes the non-linearity of viscosity with strain rate. For most of the experiments described below, we use $n = 1$, for which we write $B = 2\eta$, and η is the Newtonian viscosity coefficient. We ignore elastic strain, because the deformation that we describe occurs primarily in the lower crust and upper mantle at temperatures for which elastic strain is converted to viscous strain on timescales much shorter than those we study. Finally, we assume that the sheet is incompressible so that:

$$\nabla \cdot \mathbf{u} = e_{ii} = \frac{\partial u_i}{\partial x_i} = 0. \tag{4}$$

In eq. (4) the Einstein summation convention is used, and u_i are the components of velocity. For a two-layered medium, eqs (1)–(4) apply to each layer, and they can be solved subject to the boundary conditions that displacements and tractions are continuous across the interface between them.

For simple Rayleigh–Taylor instability the key dimensionless parameters may be obtained by dimensional analysis. For a negatively buoyant layer of thickness L, constant density ρ_1 and constant Newtonian viscosity η_1, overlying a less dense layer of density ρ_a and negligible viscosity, the (exponential) growth rate of a harmonic perturbation to the interface is proportional to $\Delta\rho g L/\eta_1$, where $\Delta\rho = \rho_1 - \rho_a$. Thus, time can be scaled to $\eta_1/\Delta\rho g L$ and distance to L. The dimensionless growth rate then depends only on the dimensionless wavenumber. Numerical experiments by Molnar *et al.* (1998) showed that inclusion of a sensible finite viscosity of the substratum (asthenosphere) reduced maximum growth rates of downwelling by only ∼20 per cent, but otherwise did not affect the instability. Nonlinear viscosity converts exponential growth to power-law growth (Canright & Morris 1993; Houseman & Molnar 1997) and adds one additional dimensionless parameter, n in (3). The form of the flow depends on the harmonic content of the perturbation, but we may assume that the fastest growing harmonic soon dominates the solution.

Adding a buoyant layer, so that the layered complex consists of three layers, crust and mantle lithosphere overlying an inviscid substratum, complicates the problem considerably, if only because it adds parameters that affect the development of the instability (Neil & Houseman 1999). A second layer with different thickness, density and viscosity adds at least three new (dimensionless) parameters that also affect the solution. Thus, perhaps it is no surprise that the pattern of flow can be very different.

Following Houseman *et al.* (2000), we carried out several series of numerical experiments on such a two-layered sheet of crust and mantle lithosphere of thickness L and horizontal length $2D_0$, undergoing horizontal shortening in the x direction. We consider only 2-D plane-strain viscous flow in the vertical plane that includes $\hat{x}$, with localized convergence forced by the following mechanical boundary conditions (Fig. 2):

$$u(x, 0) = U_0 \quad \text{for } x < (D_0 - D_1) \text{ and } u(0, z) = U_0, \tag{5a}$$

$$u(x, 0) = U_0 \sin\left(\frac{\pi(D_0 - x)}{2D_1}\right) \quad \text{for } (D_0 - D_1) \le x \le (D_0 + D_1), \tag{5b}$$

$$u(x, 0) = -U_0 \quad \text{for } x > (D_0 + D_1) \text{ and } u(2D_0, z) = -U_0. \tag{5c}$$

Here u is the horizontal component of velocity, and at least at the top surface shortening is localized in a region of width $2D_1$. Because of symmetry, we solved eqs (1)–(4) only in the range $0 \le x \le D_0$, treating $x = D_0$ as a reflecting (free-slip) boundary. To complete the set of boundary conditions, we set the vertical component of velocity $w = 0$ at the top of the crust $z = 0$ and assign vanishing shear stress to the side boundaries and vanishing vertical and horizontal tractions

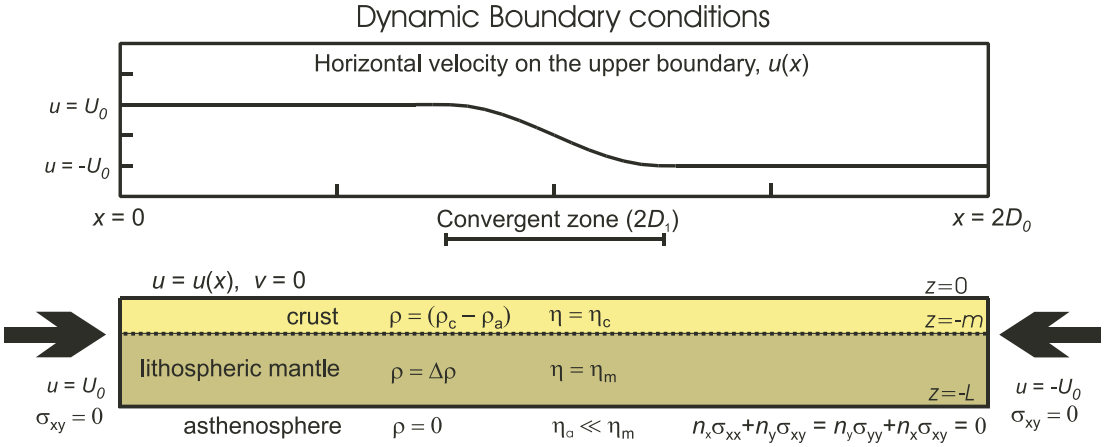

Figure 2. Schematic diagram showing the initial shape of the model lithospheric layer and boundary conditions, beneath a graph of imposed horizontal velocity versus distance along the upper surface $z = 0$ (after Houseman *et al.* 2000).

to its base (initially at $z = -L$). At $t = 0$:

$$w(x, 0) = 0 \text{ for all } x, \tag{6a}$$

$$\sigma_{xz}(0, z) = \sigma_{xz}(D_0, z) = \sigma_{xz}(2D_0, z) = 0 \text{ for all } z, \tag{6b}$$

$$\sigma_{xz}(x, -L) = \sigma_{zz}(x, -L) = 0 \text{ for all } x. \tag{6c}$$

In general, we used a sheet with $D_0 = 6L$, but for a few runs we used $D_0 = 12L$. Houseman *et al.* (2000) showed that the width of the convergent zone on the surface, $2D_1$, had little effect on results, and accordingly we carried out all experiments described here with $D_1 = L$. Setting zero traction on the base of the lithosphere (eq. 6c) is possible because we subtract a lithostatic reference column whose density everywhere is that of the asthenosphere, ρ_a. A Lagrangian frame is used for the finite-element calculations (carried out using computer program basil developed by Houseman, Barr and Evans (http://earth.leeds.ac.uk/∼greg/basil)), so that material points X_j, and boundary conditions (except 5), are advected with the flow by

$$\frac{\partial X_i}{\partial t} = u_i. \tag{7}$$

We neglect diffusion of heat and its effect on the density distribution, because we investigate instability that develops in a time which is short compared with the thermal diffusion timescale for lithosphere of thickness L. Although diffusion of heat can suppress instability at shorter wavelengths, Conrad & Molnar (1999) showed that the scaling laws developed to describe the growth of Rayleigh–Taylor instability (Houseman & Molnar 1997) carry over to convective instability.

We use displacement boundary conditions on the top surface of the model lithosphere, which prohibit vertical movement and specify horizontal movement. This choice deserves discussion because it is, in general, inconsistent with the actual stress-free condition on the Earth's surface. The alternative of using the stress-free condition on this system of 2-D homogeneous layers, however, results in a broad distribution of strain (over the entire width of our model domain) that is inconsistent with the more concentrated deformation observed in convergent belts such as in southern California (Shen *et al.* 1996), South Island, New Zealand (Beavan & Haines 2001) or the Tien Shan (Avouac *et al.* 1993).

Localization of strain may in fact be caused by along-strike variation of structure, in conjunction with a non-Newtonian lithospheric viscosity (e.g. Billen & Houseman 2004), or by initial lateral variation in strength parameter (e.g. Burov & Molnar 1998). To keep the 2-D model formulation simple, and to avoid the *ad hoc* aspect of defining arbitrary lateral variation of strength, we follow Houseman *et al.* (2000) in imposing the surface displacement rate that is consistent with observation in convergent belts. A consequence of this choice is that some aspects of the crustal flow field may be unrealistic for some parameter combinations where large surface shear tractions are implied. Nevertheless, Billen & Houseman (2004) showed that a weakening of the central convergent zone, which could result from the interaction of along-strike shear and non-Newtonian viscosity, on a system with a large crust/mantle viscosity ratio favours the development of central downwelling in all cases that they examined.

The assumption here of plane-strain deformation in the vertical plane also denies the possibility of the deformation developing a 3-D structure. The solutions that we discuss here depict the development of sheet-like structures with axes perpendicular to the orientation of convergence. In reality such structures are probably unstable to the development of along-strike disturbances that cause a downwelling sheet to evolve into a number of separate blobs.

Table 2. Parameters used to render equations dimensionless.

Quantity	Scaling	Dimensionless quantity
Distance	L	$(x', z') = \left(\frac{x}{L}, \frac{z}{L}\right); m' = \frac{m}{L}$
Density	$\Delta\rho$	$\rho'_c = \frac{\rho_c - \rho_a}{\Delta\rho}$
Viscosity coefficient*	B_1	$B'_c = \frac{B_c}{B_1}$
Time*	$\left(\frac{B_1}{\Delta\rho g L}\right)^n$	$t' = t\left(\frac{\Delta\rho g L}{B_1}\right)^n$
Speed*	$L\left(\frac{\Delta\rho g L}{B_1}\right)^n$	$U'_0 = \frac{U_0}{L}\left(\frac{B_1}{\Delta\rho g L}\right)^n$
Stress or pressure	$\Delta\rho\, gL$	$p' = \frac{p}{\Delta\rho g L}; \sigma' = \frac{\sigma}{\Delta\rho g L}$

*For Newtonian viscosity, $B = 2\eta$ and $n = 1$.

Following Houseman *et al.* (2000), we render distances dimensionless using the layer thickness, $L : (x', z') = (x/L, z/L)$, and times by $t' = t(\Delta\rho g L/B_1)^n$, where B_1 is the viscosity coefficient for the mantle lithosphere (Table 2). For Newtonian viscosity, with $B_1 = 2\eta_1$, this scaling becomes $t' = t(\Delta\rho g L/2\eta_1)$. Thus, the dimensionless convergence rate is given by

$$U'_0 = \frac{U_0}{L}\left(\frac{B_1}{\Delta\rho g L}\right)^n,$$

or for Newtonian viscosity

$$U'_0 = \frac{2\eta_1}{\Delta\rho g L^2} U_0.$$

Other key parameters are the ratio of crustal density to that of the mantle lithosphere, with both measured relative to asthenospheric density, $\rho'_c = (\rho_c - \rho_a)/\Delta\rho$, the ratio of viscosity coefficients in crust and mantle lithosphere, $B'_c = B_c/B_1$ (or $\eta'_c = \eta_c/\eta_1$), and the fraction of lithosphere that is crust, $m' = m/L$, where m is crustal thickness.

Among the parameters that Houseman *et al.* (2000) investigated, the two with the largest effects were the rate of shortening U'_0 and the viscosity ratio η'_c. They found that the rate U'_0 is the key determinant of whether gravitational instability has time to develop. They also found that if the instability develops, its form depends strongly on η'_c (see Fig. 3). Because the buoyancy of the upper lighter layer also profoundly affects the flow, we focus our experiments on assessing the effects of ρ'_c and m' on the occurrence of single versus double downwelling sheets.

RESULTS: CRUSTAL DENSITY AND THICKNESS

Based on systematic numerical experiments, we constructed phase diagrams (Figs 3–6) that separate regions in parameter space where a single downwelling (e.g. Fig. 1a) develops from those for which a pair of downwellings forms beneath the flanks of the thickest crust (e.g. Fig. 1c). Thinning of mantle lithosphere commonly occurs on either side of a central downwelling, whereas with paired downwellings, thinning occurs primarily in the central zone beneath the area of horizontal shortening. We distinguish a third, transitional, part of the phase space where the downwelling is broadened into two distinct loci, but they develop too close together for thinning to occur between them (e.g. Fig. 1b). To complete the description of this phase space, we note also that if U'_0 is too large, the gravitational instability grows slowly, and the lithosphere may be thickened everywhere, though mostly in the central zone.

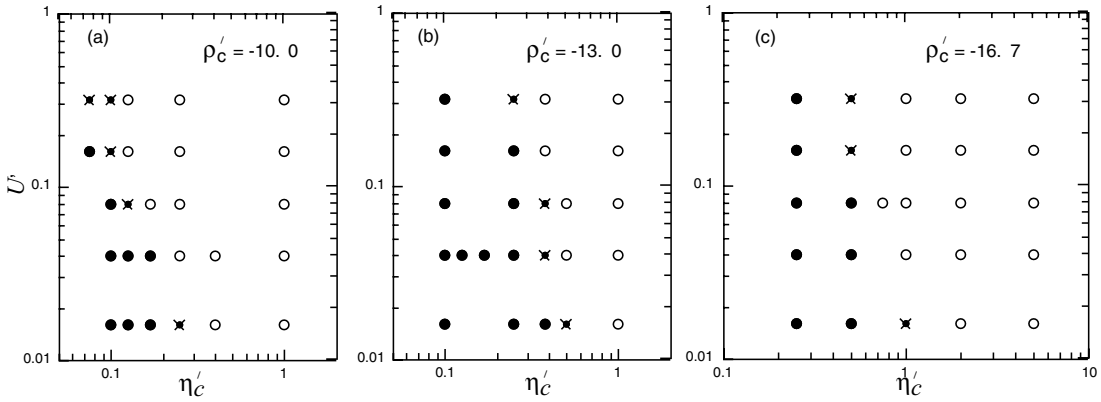

Figure 3. Phase diagram showing variations in the form of the instability in the U_0' versus η_c' plane for runs with $\rho_c' = -10.0$ (a), -13.0 (b) and -16.7 (c), $m' = 0.333$ and constant values of density and viscosity in both the crust and mantle lithosphere. Open circles show the occurrence of single downwelling beneath the thickened crust, and black circles show paired, marginal downwelling flow. Symbols with crosses indicate transitional cases where no thinning of mantle lithosphere occurred beneath the central zone.

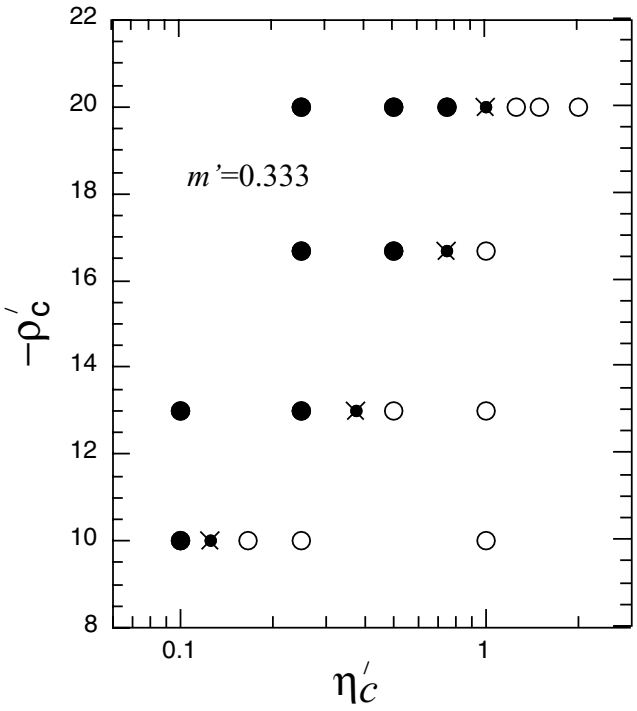

Figure 4. Phase diagram in the $-\rho_c'$ versus η_c' plane for runs with $U_0' = 0.08$, $m' = 0.333$, constant values of density and viscosity in both the crust and mantle lithosphere, showing the separation of single and paired downwellings, with symbols as in Fig. 3.

If temperature increases from ∼550 °C at the base of the crust to ∼1300 °C at the top of the convecting asthenosphere, then for a coefficient of thermal expansion of 3×10^{-5} °C^{-1}, the density should drop by 75 kg m^{-3}, corresponding to an average difference of $\Delta\rho = 37.5$ kg m^{-3} between mantle lithosphere and asthenosphere. (We ignore the effect of pressure on density, because it introduces no lateral variation in density.) With commonly assigned densities to normal continental crust of $\rho_c = 2.8$ Mg m^{-3} and to asthenosphere of $\rho_a = 3.3$ Mg m^{-3}, the dimensionless ratio of densities at the Moho is:

$$\rho_c' = \frac{\rho_c - \rho_a}{\Delta\rho} = -13.3. \quad (8)$$

Allowing for variation in the geotherm and some uncertainty in the crustal density, we carried out experiments with $\rho_c' = -10.0$, -13.0, -16.7 and -20.0. We ignore the possibility of neutrally buoyant mantle lithosphere, which might underlie Archean or early Proterozoic crust (e.g. Jordan 1981; Griffin *et al.* 1998; Kaminski & Jaupart 2000) and would prevent the instability considered here from occurring.

Different values of ρ_c' affect the transition from central downwelling beneath the thickest crust to paired downwelling beneath the edges of the thickened crust. A weak dependence on the convergence rate, U_0', characterizes the boundary between single and paired downwelling for all values of ρ_c' studied (Fig. 3; Houseman *et al.* 2000). If the density of the crust is increased relative to that of the mantle lithosphere (less negative ρ_c'), the boundary between single and paired downwellings is found at lower viscosity ratios (η_c') (Figs 3 and 4).

One might question the assumption of constant density in the mantle lithosphere, because in Earth (setting compressibility and compositional variation aside) density decreases with depth across the lithosphere. We ran several series of experiments in which the density in the crust was kept constant, but that in the mantle lithosphere decreased linearly from a value of $\rho_a + 2\Delta\rho$ at its top (initially $z = -m$), to ρ_a at the bottom (initially $z = -L$). In these experiments the density is advected with the deforming medium, and the total negative buoyancy of the mantle lithosphere is the same as that of the constant-density experiments with the same value of ρ_c'. For a given value of U_0', the boundary between single and paired downwellings occurs at values of η_c' roughly 1.3–3 times greater than for the runs with constant density (compare Figs 5 with 3 and 6b with 4). Thus, with the more realistic linearly decreasing density, marginal downwellings develop for somewhat greater crust-to-mantle-lithosphere viscosity ratios.

The results described above (Figs 3–6) show that the buoyancy of the crust plays a role as important as that of the viscosity ratio in determining whether a single downwelling forms beneath the centre of the convergent zone, or paired downwellings develop beneath the flanks. Accordingly, crustal thickness should also affect the structure of downwelling sheets. Experiments with m' between 0.25 and 0.5 (Fig. 6) show that the transition from single to paired downwelling depends strongly on m'. For relatively thick crust ($m' = 0.5$), paired downwellings can develop even when the viscosity of the crust is greater than that of the mantle lithosphere. By contrast, for crust

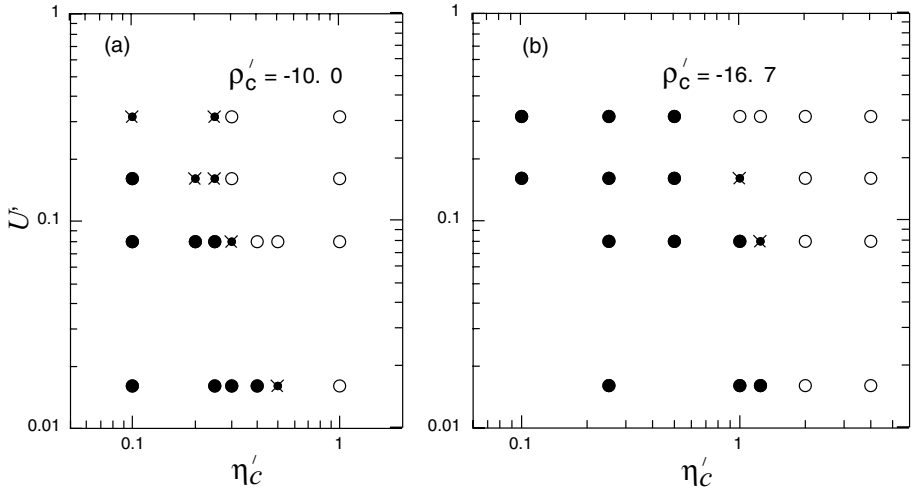

Figure 5. Phase diagram in the U_0' versus η_c' plane for runs with $\rho_c' = -10.0$ (a) and $\rho_c' = -16.7$ (b), with $m' = 0.333$, constant values of viscosity in both the crust and mantle lithosphere, and constant density in the crust, but with density decreasing linearly in the mantle lithosphere. Symbols show the separation of single and paired downwellings as in Fig. 3.

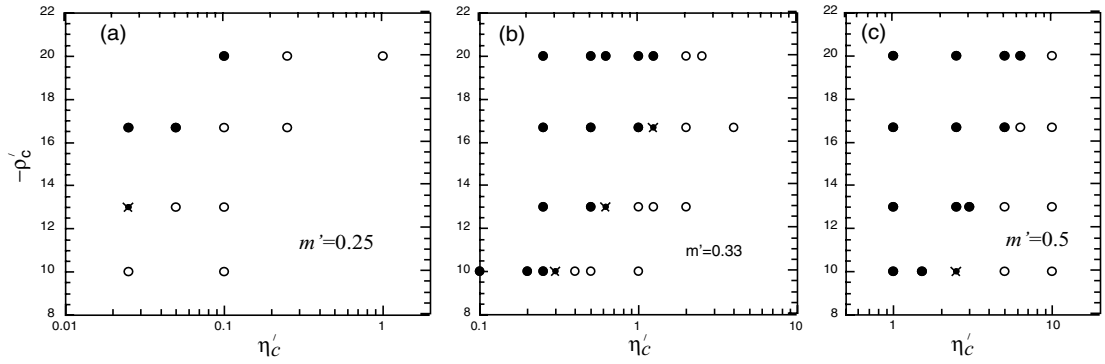

Figure 6. Phase diagram in the $-\rho_c'$ versus η_c' plane for runs with $U_0' = 0.08$, $m' = 0.25$ (a), 0.33 (b) and 0.50 (c), constant values of viscosity in the crust and mantle lithosphere, constant density in the crust, but with density decreasing linearly in the mantle lithosphere. Symbols show the separation of single and paired downwelling as in Fig. 3.

only one-quarter the thickness of the lithosphere ($m' = 0.25$), paired downwellings require a very low relative crustal viscosity, $\eta_c' < 0.1$, even at the lowest crustal densities. For runs with $m' = 1/6$ and values of η_c' as small as 0.025, only single downwellings developed beneath the thickest crust.

ANALYSIS OF LINEAR STABILITY

The response of this system to variations of viscosity, density and thickness of crust and mantle lithosphere suggests that the transition might depend on a simple scaling relationship. In an effort to find such a relationship, we analysed the stability of the layer interfaces to small perturbations, for which the governing equations can be linearized. For the Rayleigh–Taylor instability with two interfaces separating constant-density layers, two eigenfunctions, characterized by distinct growth (or decay) rates, describe flow within the layers and at their boundaries (Neil & Houseman 1999). We use the relative magnitude of these eigenfunctions to develop an approximate scaling relationship that describes the transition from central downwelling to marginal downwelling.

We assume that the externally forced convergence represented in Fig. 2 establishes a local perturbation in lithospheric and crustal thickness, and that this perturbation drives the subsequent growth or decay of the natural, buoyancy-driven eigenfunctions of the Rayleigh–Taylor instability. Thus we assume that the timescales for the externally forced convergence and the natural growth or decay rates of the instability may be separated. Furthermore, even though both eigenfunctions show maximum growth or decay rates at different spatial wavenumbers, we assume that a common wavenumber applies, because both are contributing to a single flow field. Finally, we make the usual assumption of linear theory that deflections of the interfaces are small relative to the layer thicknesses. In practice, numerical experiment has shown that small in this context means perturbations as large as approximately one-tenth of the layer thickness.

Viscous flow model

The implementation of the theory for Rayleigh–Taylor instability is well known (e.g. Chandrasekhar 1961), but for the sake of completeness, we summarize it briefly here, following the formalism used by Neil & Houseman (1999). In a stratified viscous fluid layer, in which each layer is homogeneous, the component of vertical velocity $w(x, z, t)$ resulting from eqs (1)–(4) above may be shown to satisfy

$$\nabla^4 w = 0. \tag{9}$$

We seek solutions of the form:

$$w(x, z, t) = W(z) \cos kx \exp qt \tag{10}$$

with harmonic variation in the horizontal position and exponential growth ($q > 0$) or decay ($q < 0$) in time. Substitution of (10) into (9), using quantities rendered dimensionless by the same scales defined in Table 2, yields a solution for W' of the form:

$$W'(z') = A \sinh k'z' + B \cosh k'z' + Ck'z' \sinh k'z' + Dk'z' \cosh k'z'. \tag{11}$$

Similarly, the (dimensionless) pressure, p', may be shown to satisfy

$$\nabla'^2 p' = 0. \tag{12}$$

For solutions of the form:

$$p'(x', z', t') = P'(z') \cos k'x' \exp q't' \tag{13}$$

conservation of momentum requires that

$$P'(z') = -k'(C \sinh k'z' + D \cosh k'z'). \tag{14}$$

For two homogeneous layers above an inviscid but less dense half-space, a solution consists of two functions like (11), with coefficients A_c, B_c, C_c, and D_c for the upper (crustal) layer, and A_m, B_m, C_m, and D_m for the lower layer. The determination of these eight coefficients depends on the prescription of boundary conditions. To mimic the numerical experiments that we have carried out, we assume that the perturbation has zero displacement in both vertical and horizontal directions at the top surface $z' = 0$:

$$W'_c = \frac{dW'_c}{dz'} = 0. \tag{15}$$

At the base of the layers ($z' = -1$) zero shear traction requires:

$$-k'^2 W'_m + \frac{d^2 W'_m}{dz'^2} = 0 \tag{16}$$

and a normal traction proportional to displacement, which leads to:

$$-W'_m = q' \left(P'_m + \frac{dW'_m}{dz'} \right). \tag{17}$$

At the interface between the two layers ($z' = -m'$), we assume continuity of the two components of velocity:

$$W'_c = W'_m \tag{18a}$$

$$\frac{dW'_c}{dz'} = \frac{dW'_m}{dz'} \tag{18b}$$

where (18b), like eq. (16), follows from incompressibility (4). Continuity of the two components of traction at the interface implies:

$$\eta'_c \left(-k'^2 W'_c + \frac{d^2 W'_c}{dz'^2} \right) = \left(-k'^2 W'_m + \frac{d^2 W'_m}{dz'^2} \right) \tag{19a}$$

$$-\rho'_c W' = q' \left[(P'_c - P'_m) + \left(\eta'_c \frac{dW'_c}{dz'} - \frac{dW'_m}{dz'} \right) \right]. \tag{19b}$$

Substitution of P'_c, P'_m, W'_c, and W'_m from (11) and (14) into the boundary condition eqs (15)–(19) yields an 8×8 linear matrix equation that has non-trivial solutions only if the determinant of that matrix is zero. Setting the determinant to zero gives an equation that is quadratic in the growth rate q' (because q' appears in eqs (17) and (19b)). Thus, q' has two possible values, dependent on the other physical parameters. Because the boundary between lithosphere and asthenosphere is unstably stratified, and is therefore associated with a positive growth rate, deflections from the horizontal will amplify. The stably stratified boundary between crust and mantle lithosphere, however, is associated with a negative growth rate; deflections should relax to a horizontal surface.

For a range of possible horizontal wavenumbers, we can compute the magnitudes of the growth and decay rates by solving this quadratic equation (Figs 7a and b). The velocity function for either the growing or decaying mode (Figs 7c and d) can be directly obtained from the eigenvectors corresponding to the zero eigenvalues of the 8×8 matrix, for any given $k' = kL$. We used the commercial software Mathematica to facilitate the matrix algebra. For the growing mode, the velocity eigenfunction $W'_g(z')$ is negative (downward) for an initial negative deflection of the base of the lithosphere, consistent with the growth of a gravitational instability. For the decaying mode the velocity eigenfunction $W'_d(z')$ is positive (upward) for an initial negative deflection of the Moho, consistent with the stability

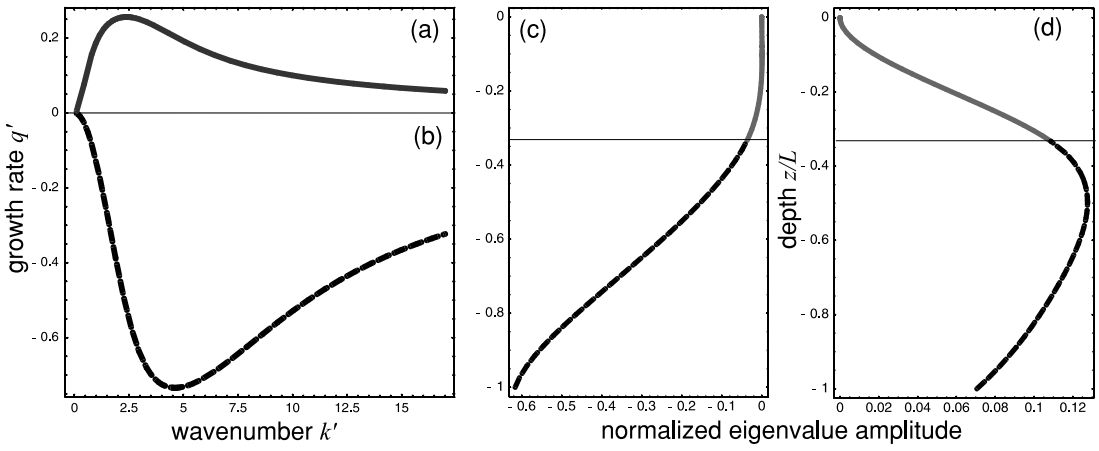

Figure 7. Dimensionless growth rate q' versus wavenumber k' (both dimensionless), calculated by using linear stability analysis (homogeneous layers, rigid upper boundary), for the positive growth rate (a) and for the negative growth rate (b) for the example case in which $m' = 0.333$, $\rho'_c = -10$ and $\eta'_c = 1$. Also shown are the vertical velocity functions $W'_g(z')$ for the growing mode (c) and $W'_d(z')$ for the decaying mode (d), both calculated at $k' = 3.317$, the geometric mean of the maximum growth and decay rates determined from (a) and (b). Those parts of the velocity function within the crustal layer are shaded lighter, and those in the mantle layer are dashed. The absolute amplitude of the eigenfunctions is arbitrary.

of this interface. For each mode, one of the density interfaces dominates the solution and drags the other along with it, opposite to the direction in which it would naturally move. The full general solution to eq. (9) for arbitrary initial deflection of the two defining surfaces would consist of an appropriate linear combination of $W'_g(z')$ and $W'_d(z')$, convolved over the wavenumber spectrum. In what follows, however, we assume that only a single harmonic is present in the initial perturbation, and we choose the dimensionless wavenumber k' to be the geometric mean of the wavenumbers of maximum growth of $W'_g(z')$ and decay of $W'_d(z')$.

Partitioning between the two modes

Consider the situation with two homogeneous layers and an initial state simply described by the amplitude of a harmonic displacement of the crust–mantle boundary, $\delta m \cos kx$, and a similar harmonic displacement of the base of the lithosphere, $\delta L \cos kx$. These two amplitude parameters determine how much of each velocity eigenfunction is present in the initial state. For an arbitrary initial deflection ratio $\delta m/\delta L$, the initial velocity solution contains both modes in the appropriate linear combination. Because growth is exponential in time, the displacement eigenfunctions $Z'(z')$ (which, added in the appropriate linear combination, provide the initial value of $\delta m/\delta L$) are simply proportional to their respective velocity eigenfunctions $W'(z')$. If the initial ratio $\delta m/\delta L$ is close to the ratio $W'(-m')/W'(-1)$ appropriate to the growing eigenfunction (e.g. Fig. 7c), the solution is dominated by the growing mode. If instead the initial condition has a deflection ratio appropriate to that of the decaying eigenfunction (e.g. Fig. 7d), the solution is dominated by the decaying mode.

In the absence of continued external forcing, exponential growth and decay imply that the solution rapidly becomes dominated by the growing term as the other term decays. For that reason the decaying term is often neglected (e.g. Neil & Houseman 1999). When an external agent (e.g. plate boundary convergence) forces deflections δm and δL, however, such forcing can continually renew the decaying mode, and as we show below, the decaying mode can overwhelm the growing mode. The sign of the growing mode can then be reversed, so that its spatial phase is shifted by half a wavelength.

External forcing

The model we use to describe the effect of convergence on crustal and lithospheric thickness assumes a constant vertical strain rate, in which vertical displacement is proportional to the original depth. Such a model is no doubt over-simplified, but is widely used, and we consider the consequences of uniformly distributed thickening on buoyancy-driven flows like those described in the previous section. A local thickening factor in the convergent zone that is proportional to depth implies:

$$\frac{\delta m}{\delta L} = m'. \tag{20}$$

Each of the displacement-rate eigenfunctions $W'_g(z')$ and $W'_d(z')$ is proportional to its respective displacement eigenfunction, $Z'_g(z')$ and $Z'_d(z')$, with proportionality constants q'_g and q'_d respectively. The forced displacement function is represented as a linear combination of the two displacement eigenfunctions:

$$Z'(z') = aZ'_d(z') + bZ'_g(z') \tag{21}$$

constrained by the assumption of depth-independent thickening rate:

$$\frac{Z'(-m')}{Z'(-1)} = \frac{\delta m}{\delta L} = m'. \tag{22}$$

The amplitude $Z'(z')$ in (21) is unconstrained (but small) in the linear theory, but the ratio a/b is significant, and may be calculated directly from (21) and (22):

$$\frac{a}{b} = \frac{m'Z'_g(-1) - Z'_g(-m')}{Z'_d(-m') - m'Z'_d(-1)}. \tag{23}$$

The amplitudes of a and b may be normalized by specifying $Z'(-1) = -1$ (e.g. Fig. 8a). From the initial perturbation described by (21), the displacement rate W' is obtained by differentiating:

$$W'(z') = W'_d(z') + W'_g(z') = aq'_dZ'_d(z') + bq'_gZ'_g(z'). \tag{24}$$

If the interface beneath the centre of convergence moves up, the assumption of a harmonic perturbation implies that it moves down on either side of the central convergent zone, thus explaining why marginal downwelling may occur if the decaying eigenfunction dominates. This method therefore offers a simple means of categorizing the behaviour of this simplified three-layer system over the relevant range of physical parameters, based on the simple criterion of whether the displacement-rate function $W'(z')$ is positive or negative at the base of the lithosphere. Because of the artificial separation of the forced component of flow from the buoyancy-driven component, however, this method provides only an approximate answer to the question of whether forced convergence will trigger central downwelling or marginal downwelling. For example, we have assumed that the rate of forced convergence is fast compared with the development of the instability and that it is independent of depth. Nevertheless, we think that this approach captures the fundamental balance of stress, includes the influence of the principal physical parameters and is broadly consistent with numerical experiments, as we show below. In cases where the Moho deflection drives a net upward flow in the convergent zone, it appears natural (with the benefit of hindsight) that the growing mode will instead produce downwelling on both sides of the convergent zone.

Dependence of the form of instability on physical parameters

For typical parameters, q'_d is negative and generally significantly greater in amplitude than q'_g, which is positive (e.g. Fig. 7). For the example in Fig. 8(b), with $\rho'_c = -10$, $m' = 1/3$, and $\eta'_c = 1$, we see that the externally driven convergence induces an internal flow field in which the Moho and most of the lithospheric mantle move upwards, driven by the relaxation of the Moho deflection, while only the lowermost part of the lithosphere moves downwards.

Before we attempt to generalize the results of these calculations, let us discuss some other specific examples that illustrate the effects of the key physical parameters. The effect of relative crustal density is anticipated from the numerical experiments (Figs 4 and 6); a relatively low-density crust (more negative value of ρ'_c) drives the relaxation of the Moho more strongly, and the growing mode will be relatively weaker in the composite solution. Comparing Figs 8(d) and (b), a decrease in ρ'_c from -10 to -20 suffices to reverse the direction of flow at the base of the lithosphere from downwelling to upwelling, thus illustrating the transition from central downwelling to marginal downwelling as the density parameter is varied.

As Houseman *et al.* (2000) showed, the effect of increasing the relative strength of the crust is to enhance central downwelling. Compared with $\eta'_c = 1$ (Figs 8a and b), a greater crustal strength, such as $\eta'_c = 5$, has the effect of suppressing crustal flow in the growing mode (Figs 9a and b).Because the magnitude of the decay rate q'_d is reduced, the contribution of the decaying mode to the flow field is decreased. Most of the thickness of the mantle lithosphere

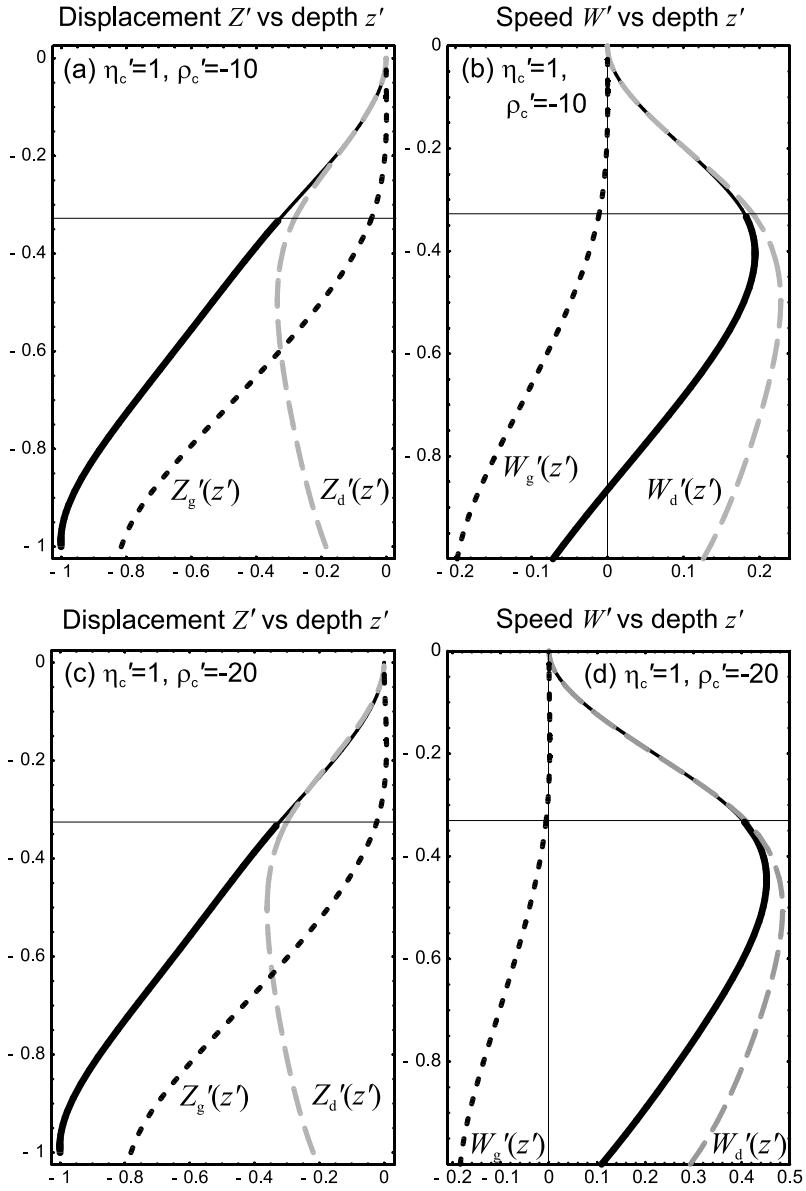

Figure 8. Normalized eigenfunctions for vertical displacement (a, c) and speed (b, d). Dashed lines show the separate displacement and speed functions for growing, $Z'_g(z')$, $W'_g(z')$, and decaying, $Z'_d(z')$, $W'_d(z')$, modes; solid lines show the total displacement and vertical speed functions obtained by addition of the two eigenfunctions. The amplitude of the total displacement is normalized to -1 at the base of the lithosphere; other amplitudes follow from eqs (21–24). For the two calculations shown here $m' = 0.333$ and $\eta'_c = 1$. For (a) and (b) $\rho'_c = -10$ and $k' = 3.317$ (as for Fig. 7); for (c) and (d) $\rho'_c = -20$ and $k' = 3.404$.

moves down, despite the upward relaxation of the Moho (Fig. 9b). Central downwelling, predicted here, is also observed in the numerical experiments (e.g. Fig. 3). If the crust is relatively weak (e.g. $\eta'_c = 0.2$), then the relaxation of the Moho dominates the resulting flow field (Figs 9c and d) and central upwelling (marginal downwelling) is predicted at the base of the lithosphere, as seen in the numerical experiments.

To define the general dependence of the form of downwelling on the governing physical variables, m', ρ'_c and η'_c, let us use the ratio $R = -W'_d(-1)\ W'_g(-1)$, and note that $R > 1$ defines central upwelling and $R < 1$ defines central downwelling. Using the eigenfunction method described above, we then calculated R for a broad range of parameters, varying one at a time. We sought power-law dependences of R on each of the governing parameters m', ρ'_c and η'_c by using log–log plots from which the apparent power-law index of each variable can be estimated separately, by holding the other two variables constant. Combining these separate approximate power-law dependences, we obtained the approximate empirical functional relation shown by Fig. 10:

$$R \propto m'^4 \left(\rho_c'^6 \eta_c'^{-4}\right)^{1/5} \tag{25}$$

with proportionality constant 2.8 ± 0.6. Thus, we infer that forced convergence should cause marginal downwelling to develop instead of central downwelling if $R > 1$, or if

$$m'^4 \left(\rho_c'^6 \eta_c'^{-4}\right)^{1/5} > 0.35 \pm 0.06. \tag{26}$$

Using the 2-D finite-element calculations of finite-amplitude growth, we may test (26) by plotting $\log(m'^4 \rho_c'^{6/5})$ versus $\log(\eta'_c)$

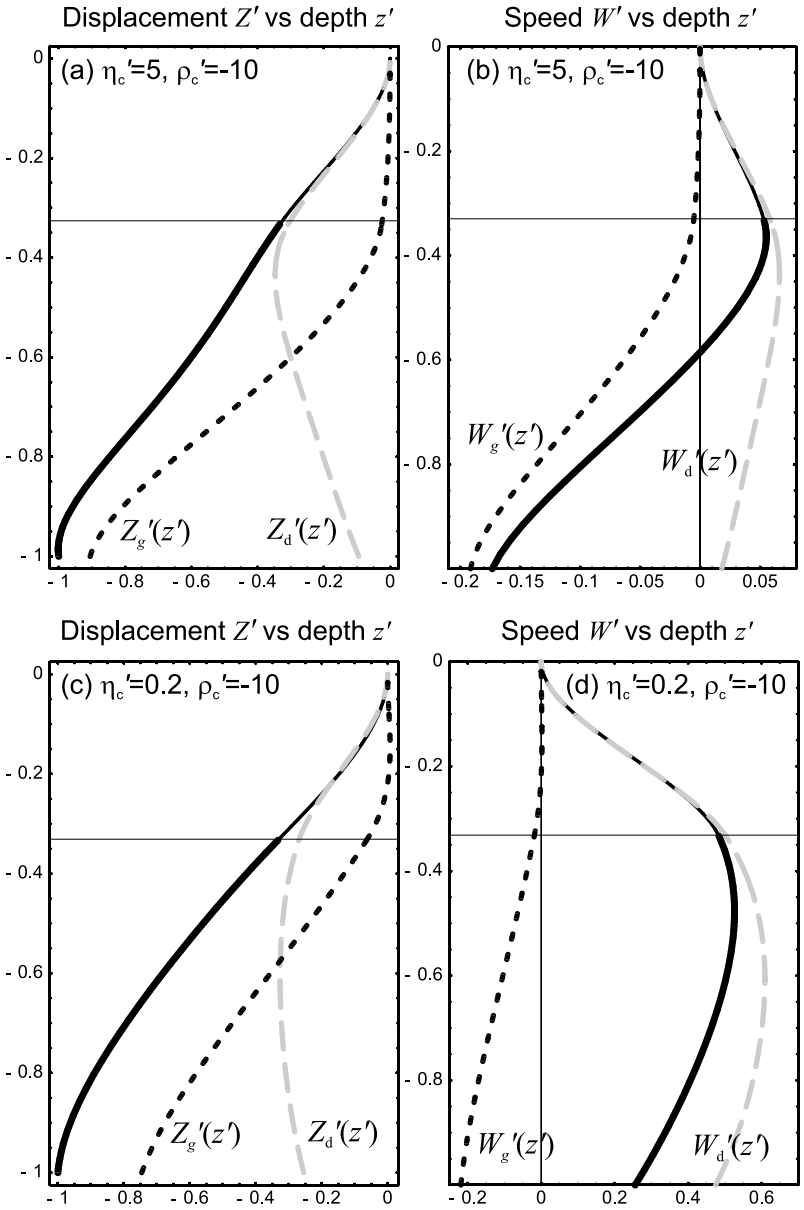

Figure 9. Eigenfunctions for vertical displacement (a, c) and speed (b, d) for experiments in which the crustal viscosity is varied. Symbols as in Fig. 8; $m' = 0.333$, $\rho_c' = -10$. For (a) and (b) $\eta_c' = 5$, and $k' = 4.107$; for (c) and (d) $\eta_c' = 0.2$, and $k' = 2.373$.

for numerical experiments carried out at a constant convergence rate (Fig. 11). If the approximate linear theory is correct, a separation between single central downwelling and paired marginal downwellings should be defined on this phase diagram by a straight line of slope $4/5$. In fact, the finite-element calculations do show an approximate separation (Fig. 11) similar to that predicted by (26), but the slope of a transition line that would be inferred from the range of data on this graph is consistent with the index for η_c' being closer to $2/3$ than $4/5$.

Several assumptions or approximations leading to (26) may contribute to the imperfect agreement between the approximate linear theory and the finite-element experiments. First, the assumption of forced convergence producing interface deflection proportional to depth (22) is not precise for the 2-D flow field used in the finite-element calculations; the amplitude ratio $\delta m/\delta L$ may be greater than m', and the wavelengths of the deflections of the two boundaries may also differ. Second, to evaluate the relative amplitudes of the growing and decaying modes in the linearized problem, we assumed an average wavenumber, although faster growth and decay rates may occur at other wavenumbers. Accordingly, we may have underestimated the response of one or the other mode in some cases. The largest differences between wavenumbers of maximum growth and decay occur for the smallest values of η_c', which is where the misfit between linear theory and numerical experiments in Fig. 11 is worst. Third, the numerical experiments show a clear dependence on convergence rate, which the linear theory does not account for. The variation of convergence rate (relative to growth rates) may be significant in explaining why some of the data points on Fig. 11 appear to fall on the wrong side of a clean transition line. Finally, the numerical experiments allow finite amplitude growth. Non-linearity associated with finite amplitude growth may allow the solution to evolve on a different path from that predicted by the

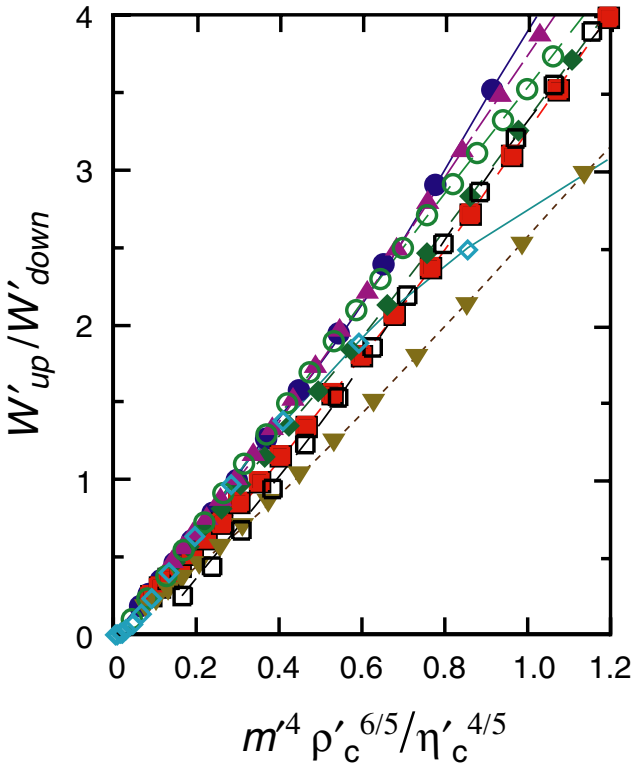

Figure 10. Graph of the ratio $R = -W'_d(-1)/W'_g(-1)$ versus the dimensionless parameter defined in eq. (25). These calculations reveal an approximate scaling relationship that holds for a broad range of parameter values. Points are coded as follows: solid blue circles, $\rho'_c = -10$, $\eta'_c = 1$, $0.25 < m' < 0.49$; solid red squares, $\rho'_c = -10$, $\eta'_c = 0.2$, $0.2 < m' < 0.38$; dark green diamonds, $\rho'_c = -15$, $\eta'_c = 0.2$, $0.2 < m' < 0.33$; upward pointing magenta triangles, $\rho'_c = -20$, $\eta'_c = 1$, $0.25 < m' < 0.41$; downward pointing yellow-brown triangles, $\rho'_c = -20$, $\eta'_c = 5$, $0.3 < m' < 0.7$; open green circles, $-3 > \rho'_c > -43$, $\eta'_c = 1$, $m' = 0.333$; open black squares, $-3 > \rho'_c > -15$, $\eta'_c = 0.2$, $m' = 0.333$; open cyan diamonds, $\rho'_c = -10$, $0.1 < \eta'_c < 100$, $m' = 0.333$.

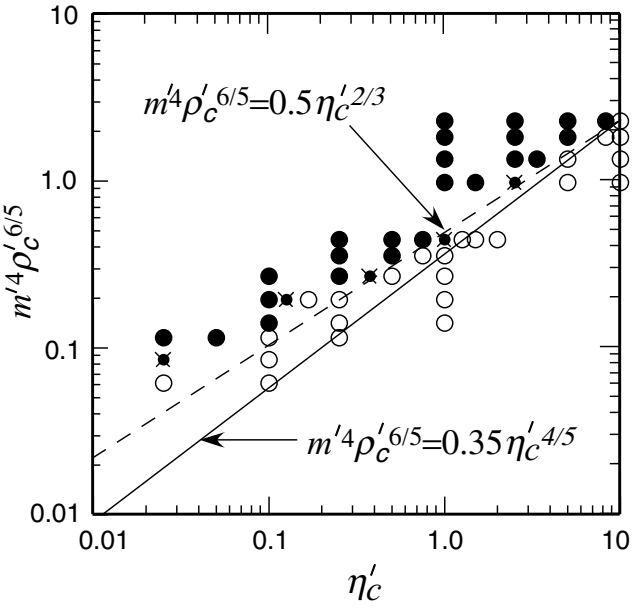

Figure 11. Phase diagram in the $m'^4\rho_c'^{6/5}$ versus η'_c plane for numerical experiments carried out at a constant convergence rate $U'_0 = 0.08$, with constant values of viscosity and density in the crust and mantle lithosphere, showing the separation of single and paired downwellings (symbols as in Fig. 3). The solid line, given by eq. (26), $m'^4(\rho_c'^6\eta_c'^{-4})^{1/5} = 0.35$, is based on the approximate linear theory; the dashed line shows the best-fit separation line for the upper range of these data: $m'^4\rho_c'^{6/5} = 0.5\eta_c'^{2/3}$.

linearized theory. Allowing for these difficulties, the approximate agreement (within a factor of 2 or so) between these two independent methods of analysis (Fig. 11) shows that (26) may be used as a guide to understanding the development of downwelling in a zone of forced convergence where crust and lithospheric mantle are laterally homogeneous.

RESULTS: DEPTH-DEPENDENT AND NON-NEWTONIAN VISCOSITY

Because of its strong temperature dependence, viscosity (or rheological strength, however it is measured) decreases with depth in the mantle lithosphere, and many presume that it decreases with depth in the crust (below an upper brittle layer). Accordingly, we carried out experiments in which the viscosity initially decreases exponentially with depth through both the crust and mantle lithosphere (viscosity like density is advected with the flow). We made a series of calculations (Fig. 12) with different values of U'_0 and initial viscosity profiles for which the viscosity variation across each of the crust and mantle layers is a factor of either 10 or 30 (dimensionless viscosity at the top of the crust is η'_c times that at the top of the mantle). If we normalize the viscosity profile so that the mean viscosity of the mantle lithosphere is 1 ($\eta'_{top} = 2.56$ or 3.52 for factors of 10 or 30 respectively, with η'_{top} equal to the dimensionless viscosity at the top of the mantle lithosphere), the resulting line of separation between single and paired downwellings occurs at values of η'_c greater by a factor of about 2 than those for constant viscosity and other similar parameters (compare Figs 12 and 3c). Within a numerical factor of ~2, the development of single or multiple downwellings may therefore still be predicted using a relation like (26) provided that depth-averaged layer viscosities are used to derive the value of η'_c. Our tests, however, have covered a relatively small range of viscosity variation and the possibility remains that an especially low viscosity in the lower crust may have a profound effect on the flow.

Houseman *et al.* (2000) presented a few calculations with non-Newtonian viscosity that showed the same general pattern of paired downwellings for relatively weak crust and a single downwelling for relatively strong crust. In examining the parameter space more thoroughly, we find the same general trends in phase space for non-Newtonian viscosity ($n = 3$; Figs 13 and 14) as for Newtonian viscosity ($n = 1$; Figs 3c and 4). For both $n = 3$ (Fig. 13) and $n = 1$ (Fig. 3c) a ratio of viscosity coefficient for crust and mantle lithosphere of approximately 1 separates paired and single downwellings for $\rho'_c = -16.7$. Moreover, for smaller crustal densities (more negative ρ'_c), paired downwellings may occur at greater values of B'_c (Fig. 14), as for Newtonian viscosity (Figs 4 and 6b). We conclude that, for 2-D plane-strain deformation, non-Newtonian viscosity does not profoundly affect the pattern of downwelling determined for Newtonian viscosity. Perhaps this is no surprise because when forced by shortening at a constant rate, the layer with non-Newtonian viscosity behaves as a Newtonian viscous fluid (with spatially variable viscosity), until growth becomes large enough that strain rates due to flow driven by gravity become comparable with those forced by convergence (e.g. Molnar *et al.* 1998).

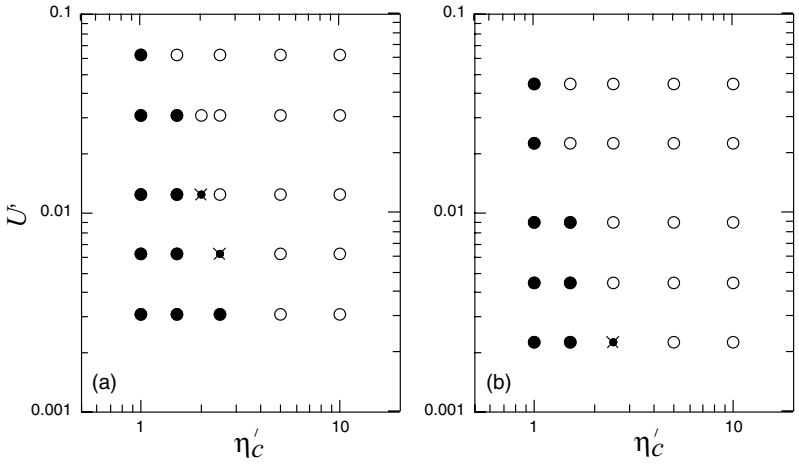

Figure 12. Phase diagram in the U_0' versus η_c' plane showing the separation of single and paired downwellings for runs with $\rho_c' = -16.7$, $m' = 0.333$, a constant value of density in the crust and the mantle lithosphere, and exponentially decreasing viscosity in both crust and mantle lithosphere such that the range of variation across each is 10 times (a) and 30 times (b). Here the value of U_0' is scaled as in Table 1, but using the mean viscosity of the mantle lithosphere in place of η_1. Symbols as in Fig. 3.

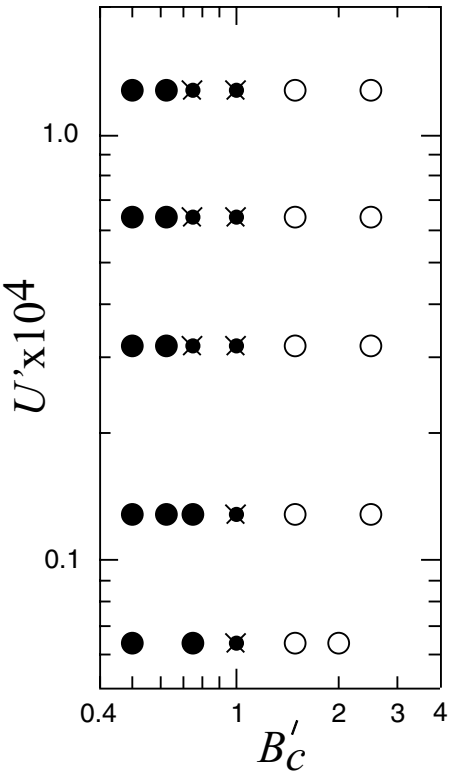

Figure 13. Phase diagram in the U_0' versus B_c' plane showing the separation of single and paired downwellings for runs with non-Newtonian viscosity ($n = 3$), $\rho_c' = -16.7$, $m' = 0.333$, and constant values of density and viscosity coefficient in both crust and mantle lithosphere. Compare this with Fig. 3(c) showing the same for Newtonian viscosity ($n = 1$). Symbols as in Fig. 3.

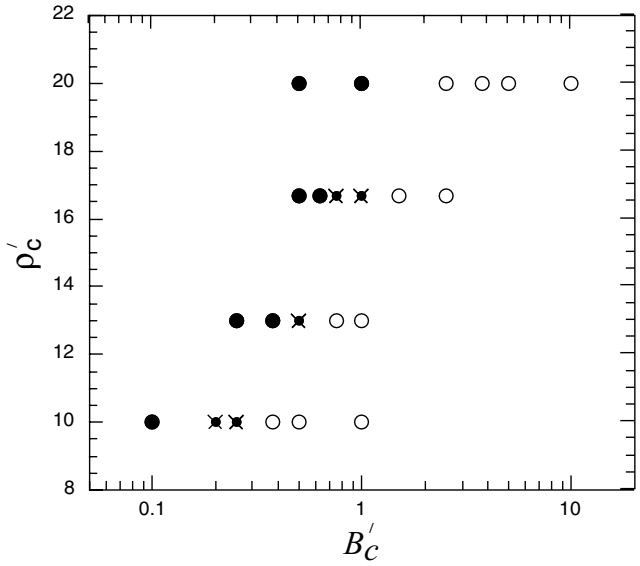

Figure 14. Phase diagram in the ρ_c' versus B_c' plane for runs with non-Newtonian viscosity ($n = 3$), $U_0' = 3.2 \times 10^{-5}$, $m' = 0.333$, and constant values of density and viscosity coefficient in both crust and mantle lithosphere, showing the separation of single and paired downwellings. Compare this with Fig. 4 showing the same for Newtonian viscosity ($n = 1$). Symbols as in Fig. 3.

DISCUSSION AND IMPLICATIONS

The difference between a single downwelling, possibly flanked by lithospheric thinning, and paired downwellings flanking a central region of lithospheric thinning should be apparent at the Earth's surface, even if hidden beneath the complexity of a crustal convergent belt. In particular, in the former situation, the weight of thickening cold mantle lithosphere driving the downwelling flow might sustain a relatively low mountain range above relatively thick crust. Conversely, where marginal downwellings develop, relatively thin crust beneath the centre of convergence would be underlain by thin mantle lithosphere and hot upper mantle that may support high topography. Moreover, the thinning of mantle lithosphere that occurs in the latter process is more likely to produce volcanism than if a single downwelling underlies the axis of convergence.

Among the parameters that we examined, the convergence rate across a deforming region has relatively little effect on the form of downwelling flow beneath the region, provided it is sufficiently slow to allow a Rayleigh–Taylor-like instability to grow. For cases with Newtonian viscosity, an order of magnitude increase in the

dimensionless convergence rate shifts the field of single downwellings to crust-to-mantle-lithosphere viscosity ratios that are only about two times lower (Figs 3, 5 and 12). For non-Newtonian viscosity, the dependence on convergence rate is yet smaller and almost negligible (Fig. 13). We should bear in mind, however, that if the forced convergence is fast relative to the viscous response time of the lithosphere, the form of downwelling will be forced by boundary conditions rather than by the buoyancy driven instability that we have discussed (Conrad 2000). In practice this condition implies that a relatively weak lithospheric mantle is required for the gravitational instability to develop as quickly as inferred for the geological examples discussed below (Houseman *et al.* 2000).

If gravitational instability occurs, the viscosity ratio between crust and mantle lithosphere is one key determinant of whether single downwellings beneath the axis of convergence occur, or paired downwellings develop on the margins of the convergent zone. Variability in η_c' is most likely to be caused by variation in effective mantle viscosity, due to the strong dependence of olivine deformation mechanisms on temperature, and the presence or absence of hydrogen (e.g. Hirth & Kohlstedt 1996). The transition, however, also depends strongly on the buoyancy of the crust. If the crust is more buoyant, it must also have a greater viscosity (relative to the mantle) for single downwelling flow to occur. Crustal buoyancy is enhanced by either greater thickness (m') or by lower density (more negative ρ_c'), both defined relative to mantle parameters.

We discussed above the likely values of the density parameter ρ_c' given in (8), based on the assumption that only temperature affects the density structure of the mantle. With typical crustal thicknesses of 35–40 km where recent deformation has not occurred (e.g. Mooney *et al.* 1998) and estimates of continental lithospheric thicknesses, outside Archean and early Proterozoic shields, ranging from 50 to 200 km (e.g. Sclater & Francheteau 1970; Sclater *et al.* 1981; Jaupart *et al.* 1998), m' may vary from about 0.5 or greater in regions with initially warm upper mantle to values less than 0.25 in old, cold stable regions where lithospheric thicknesses would be large (about 150–200 km). For lithospheric thickness of 100–120 km, $m' \approx 1/3$, and we take this as a representative value for younger continental lithosphere. The ratios of viscosity, η_c', that separate single and paired downwellings differ by nearly two orders of magnitude as m' varies from 0.25 to 0.333 to 0.5 (Fig. 6).

Single downwellings appear to underlie two regions where neighbouring, undeformed crust is relatively thin: the Southern Alps of New Zealand (e.g. Stern *et al.* 2000; Kohler & Eberhart-Phillips 2002) and the Western Transverse Ranges of California (e.g. Raikes 1980; Humphreys *et al.* 1984; Humphreys & Clayton 1990; Kohler 1999). In both regions, the surrounding crust is only ∼30 km thick (Mooney & Weaver 1989; Davey *et al.* 1998). If lithospheric strength is laterally invariant, the form of downwelling in both may be attributed to a relatively small value of m' or to a relatively large value of η_c' in order that these examples plot to the lower right of the transition shown on Fig. 11. The attribute of central downwelling could, however, also be due to lithospheric weakening in the central convergent zone, as considered by Billen & Houseman (2004).

The Kyrgyz Tien Shan in Central Asia (Fig. 15) offers an example of a region where lithosphere may have been atypically thin when crustal shortening began, and hence where m' was unusually large. Sporadic basaltic volcanism occurred in the region of the present-day Kyrgyz Tien Shan, east of the Talas–Ferghana Fault and within the present-day high terrain, from ∼120 Ma to perhaps as recently as 20 Ma (Sobel & Arnaud 2000). Thus, the upper mantle appears to have been atypically warm before ∼11 Ma, when widespread deformation seems to have begun (e.g. Abdrakhmatov *et al.* 2001; Bullen *et al.* 2001). North–south intracontinental convergence across the area roughly 300 km wide (Fig. 15b) is rapid, ∼20 mm yr^{-1} (Abdrakhmatov *et al.* 1996; Reigber *et al.* 2001). The crust beneath large basins within the Tien Shan, where elevations are relatively low, is not as thick as Airy isostasy would imply, but comparable to that in the adjacent, undeformed region north and south of the belt (Oreshin *et al.* 2002). Both low *P*-wave (Vinnik & Saipbekova 1984; Roecker *et al.* 1993) and low *S*-wave speeds (Oreshin *et al.* 2002) east of the Talas–Ferghana Fault suggest, however, relatively warm, low-density uppermost mantle that compensates for a thin crustal root (Fig. 15b). Evidence for marginal downwelling flow on either the northern or southern flank of the belt remains inconclusive, but the low-speed, low-density uppermost mantle beneath a region with such rapid surface convergence accords with the type of flow field depicted in Fig. 1(c).

The Alboran Sea and its surroundings provide another region for which there is clear evidence of lithospheric thinning in the centre of a convergent belt (Fig. 16). Late Cretaceous and early Cenozoic convergence between Europe and Africa apparently built a mountain belt that spanned the region between southern Spain and North Africa, but whose remnants today, the Betic Cordillera in southern Spain and the Rif in northern Morocco, are separated by the Alboran Sea (e.g. Doublas & Oyarzun 1989; Platt & Vissers 1989; Platt *et al.* 1998). Images of the upper mantle consistently show a high-speed zone beneath the Betic Cordillera in Spain (Blanco & Spakman 1993; Plomerovà *et al.* 1993; Spakman *et al.* 1993; Seber *et al.* 1996a,b; Bijwaard *et al.* 1998; Calvert *et al.* 2000). In most such images, the relatively high speeds are clearest below ∼100 km, which might suggest that the cold material has detached from the lithosphere above it. Images of the upper mantle beneath the Rif also suggest high-speed material but are less definitive than those for southern Spain (e.g. Seber *et al.* 1996b; Calvert *et al.* 2000). The occurrence of intermediate-depth earthquakes, however, supports the contention that cold material extends to depths greater than 100 km, and perhaps 200 km beneath northern Morocco (Hatzfeld & Frogneux 1981; Seber *et al.* 1996a; Calvert *et al.* 2000). In summary, the seismological evidence is consistent with downwelling beneath the margins of a Cenozoic convergent belt. In contrast, low upper mantle *P*-wave speeds (7.5–7.0 km s^{-1}) in the uppermost mantle beneath the Alboran Sea (Hatzfeld & Ben Sari 1977; Working Group 1978; Banda 1988) and high attenuation of shear waves (Seber *et al.* 1996a) imply thinned lithosphere and high temperatures at shallow depths in the middle of this convergent zone.

Late Cenozoic volcanism in the Alboran Sea provides further evidence for lithospheric thinning following crustal thickening. Turner *et al.* (1999) used analyses of both rare earth elements and isotopic ratios ($^{87}Sr/^{86}Sr$ and $^{143}Nd/^{144}Nd$) to argue for different sources of magma. In particular, they suggested that magmas emplaced before lithospheric thinning occurred were derived from the asthenosphere, but those emplaced ∼10 Myr after thinning began represent melting of lithosphere. In the context of our study, the earlier magmas would have formed as lithospheric mantle thinned during convergence, before widespread crustal extension and extreme thinning of mantle lithosphere occurred.

The suggestion that paired downwellings developed beneath the Rif and Betic Cordillera as lithospheric extension occurred in the lithosphere of the Alboran Sea basin is necessarily incomplete because of two observations. First, approximating the upper mantle structure as 2-D is imperfect; intermediate depth seismicity, as well as a zone of high-speed upper mantle, dip eastward beneath the region west of the Alboran Sea (e.g. Seber *et al.* 1996a,b; Calvert *et al.* 2000), which some interpret to show a westward migration of

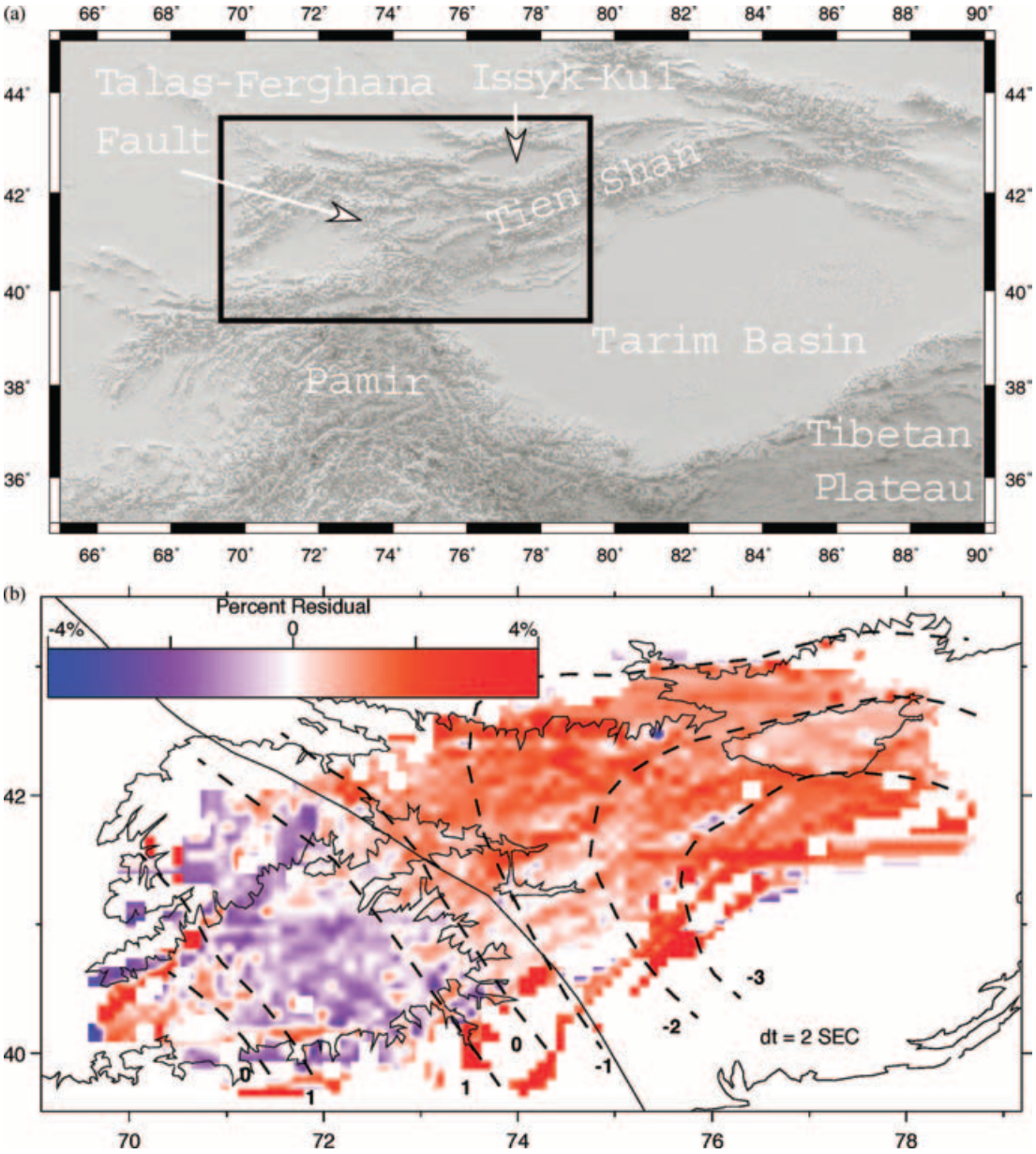

Figure 15. (a) Location map showing topography of the Tien Shan region, with the box outlining the area shown in (b). (b) Lateral heterogeneity in *P*-wave speeds in the upper mantle of the Kyrgyz Tien Shan and adjacent territory from Roecker *et al.* (1993). Colours show per cent traveltime residuals of $(\Delta t/t)$ for *Pn* ray paths in the upper mantle beneath the Tien Shan, determined by assigning a per cent residual to the part of the *Pn* ray path in the upper mantle and taking an average over all rays that pass through a unit area. Per cent residuals correspond roughly to the negative of the perturbation in wave speed required to eliminate them ($\Delta t/t = -\Delta v/v$). In dark blue (red) areas, *P*-wave speeds are up to 4 per cent faster (slower) than average. Dashed lines show contours (in per cent) of perturbations of *P*-wave speeds determined by Vinnik & Saipbekova (1984) from teleseismic arrival times. Also shown in (a) are the outline of the 1500 m elevation contour, the shore of Lake Issyk-Kul, and the trace of the Talas–Ferghana Fault, whose location is shown in (a). Note that the western boundary between the regions of low and high speeds approximately follows the position of this fault. (S. W. Roecker (personal communication, 2002) prepared this figure from the data used by Roecker *et al.* (1993).)

an eastward subducting slab (e.g. Tapponnier 1977; Royden 1993; Gutscher *et al.* 2002). Second, rapid crustal thinning and extension at ∼18–20 Ma with attendant subsidence to form the Alboran Sea (Platt *et al.* 1996, 1998; Soto & Platt 1998) left such a strong imprint on the geological record and the present-day upper mantle structure that inferring the crustal and upper mantle structure before extension began must be speculative. Thus, although the idea of marginal downwelling induced by forced convergence provides a dynamically consistent explanation for the geological evolution of this region, other explanations may be possible. The form of lithospheric instability inferred for the Alboran Sea Basin and for the western Tien Shan implies either a larger initial value of m' or a smaller value of η'_c, in order to plot these examples on the upper left of Fig. 11.

The contrast between the western Tien Shan and the Alboran Sea basin on the one hand, and the South Island of New Zealand and the Transverse Ranges of Southern California on the other hand calls attention to the range of possible evolutions of zones of continental

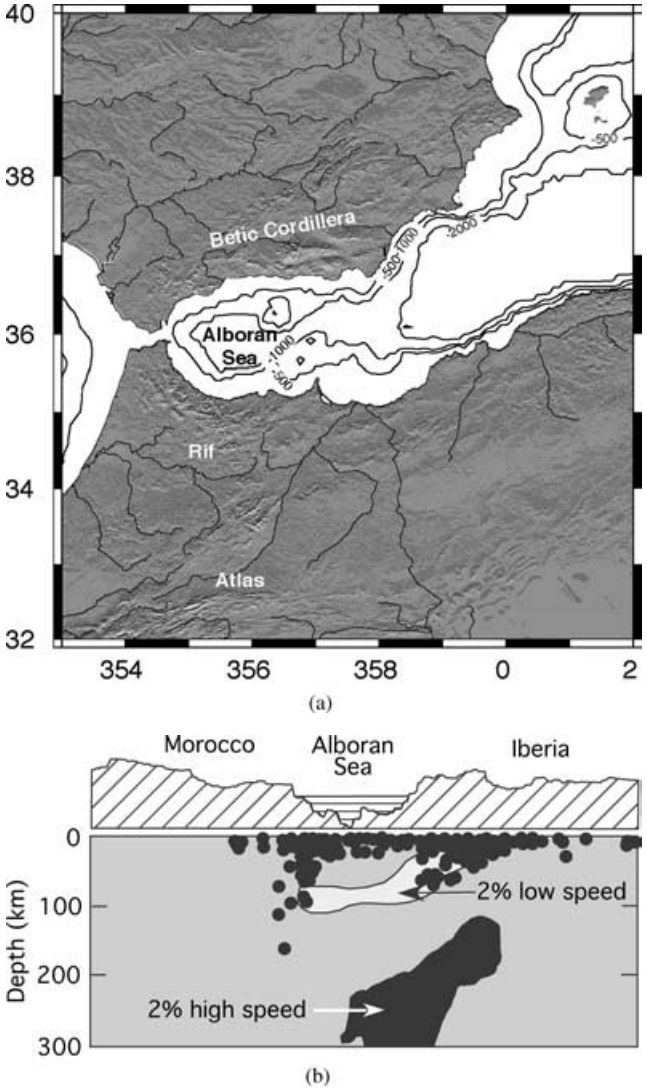

Figure 16. (a) Location map showing the Alboran Sea and adjacent Betic Cordillera and Rif mountain belts, where thrust faulting and folding developed before crustal thinning created the basin now occupied by the Alboran Sea. (b) North–south cross-section of seismic wave speeds across the Alboran Sea region, modified from Calvert *et al.* (2000). Note the high-speed regions flanking the Alboran Sea and the low-speed region directly beneath it.

convergence. In all of these cases, we think that lithospheric instability has been triggered by tectonic convergence, absorbed over a relatively small geographical region, hundreds of kilometres in horizontal dimension. Differences in the form of lithospheric instability that has occurred in these different regions may be attributed to relatively small differences in the values of m', ρ_c' or η_c' that determine whether the region of convergence is in the domain of central downwelling or marginal downwelling.

If we use the estimate of $\rho_c' = -13.3$ obtained earlier (8), and the relation (26) based on both linear stability and the numerical experiments discussed above, then we may infer from the observations of the western Tien Shan and the Alboran Sea basin that in these regions $m' > 0.35\eta_c'^{1/5}$. The opposite evidently applies to the South Island of New Zealand and the Transverse Ranges of California. The numerical coefficient is clearly uncertain to some small factor of order 1, and this conclusion could be undermined if the underlying assumptions of initially plane laterally homogeneous layers and forced 2-D plane-strain convergence were not valid.

CONCLUSIONS

The numerical experiments described above show that several gestures toward reality do not change the basic results obtained by Houseman *et al.* (2000) for an incompressible layered structure undergoing horizontal shortening. For sufficiently weak and buoyant crust (compared with mantle lithosphere), the Rayleigh–Taylor instability of the relatively dense mantle lithosphere should grow by paired downwellings beneath the flanks of the region where crustal shortening and thickening are localized, instead of by a single downwelling underlying the thickest crust. One key parameter determining which flow pattern develops is the ratio of crustal to mantle viscosity coefficient. Layers characterized by non-Newtonian ($n = 3$) viscosity behave similarly to those with Newtonian viscosity, with relatively large crust-to-mantle strength ratios associated with single downwellings and small ratios with paired, marginal downwellings. The allowance for density to decrease with depth in the mantle lithosphere, as it should in Earth because of increasing temperature (ignoring the effect of increasing pressure), shifts the boundary between single and paired downwellings toward higher crust-to-mantle strength ratios, but by less than a factor of 2. Nor do vertical variations in viscosity change these results, at least if the variations are not too large and if the depth-averaged layer viscosities are used in the formulae.

Apparently as important as the ratio of strengths of the crust and mantle lithosphere in separating single and paired downwellings is the difference between the buoyancy of the crust and the negative buoyancy of the mantle lithosphere. In affecting the transition between single and paired downwellings, increased buoyancy of the crust, due either to a lower density (compared with that of mantle lithosphere) or to increased thickness, trades off against a greater crust-to-mantle-lithosphere viscosity ratio. Relatively thick, low-density crust favours paired, marginal downwellings and lithospheric thinning between them. These relationships are encapsulated by the empirical relation shown on Fig. 11 that approximately defines the transition from single central downwelling to marginal downwelling:

$$m'^4 \rho_c'^{6/5} > 0.5\eta_c'^{2/3} \tag{27}$$

For Earth, single downwellings should develop beneath regions of active convergence either where crust is a small fraction of the lithosphere (because it is unusually thin or the mantle lithosphere is thick) or where the mantle lithosphere is unusually weak (presumably because of elevated temperatures or hydration). The inference of central downwelling is consistent, however, with the lack of volcanism in some zones of intracontinental convergence and specifically the Western Transverse Ranges of California and the Southern Alps of New Zealand, where seismological studies suggest the presence of high-speed zones beneath the ranges.

The propensity for paired, marginal downwelling flow to develop beneath regions with relatively thick, low-density crust (or relatively thin mantle lithosphere), as is inferred to have occurred beneath the western Tien Shan and the Alboran Sea basin, may offer the solution to a puzzle. On the one hand, volcanism is a common by-product of mountain building, but thickening of lithosphere should advect low-temperature material downwards and therefore inhibit volcanism. On the other hand, weak, and therefore thin, lithosphere is obviously more susceptible to intracontinental deformation than

is cold, thick lithosphere. Thus, if intracontinental belts should develop where pre-existing lithosphere is weak, why does convergence acting on the thin, weak lithosphere not simply transform it into thicker lithosphere like that adjacent to it? In the context of convective instability triggered by forced convergence, however, relatively thin lithosphere favours the development of paired marginal downwellings. While undergoing horizontal shortening, the underlying mantle lithosphere may thus be swept into marginal downwellings and thin further. By such a process, tectonic rejuvenation of initially thin lithosphere may sustain both a weak zone and one with the potential for volcanism.

ACKNOWLEDGMENTS

We thank E. Kaminsky, Y. Ricard and an anonymous reviewer for thoughtful and constructive reviews, and S. W. Roecker for constructing Fig. 15(b) for us. This research was supported in part by the National Science Foundation under grant EAR-0106909.

REFERENCES

Abdrakhmatov, K.Ye. *et al.,* 1996. Relatively recent construction of the Tien Shan inferred from GPS measurements of present-day crustal deformation rates, *Nature,* **384,** 450–453.

Abdrakhmatov, K.E., Weldon, R., Thompson, S., Burbank, D., Rubin, Ch., Miller, M. & Molnar, P., 2001. Origin, direction, and rate of modern compression in the central Tien Shan, Kyrgyzstan, *Geol. Geofiz. (Russian Geol. Geophys.),* **42,** 1585–1609.

Arnaud, N.O., Vidal, Ph., Tapponnier, P., Matte, Ph. & Deng, W.M., 1992. The high K_2O volcanism of northwestern Tibet: geochemistry and tectonic implications, *Earth planet. Sci. Lett.,* **111,** 351–367.

Avouac, J.P., Tapponnier, P., Bai, M., You, H. & Wang, G., 1993. Active thrusting and folding along the northern Tien Shan, and Late Cenozoic rotation of the Tarim relative to Dzungaria and Kazakhstan, *J. geophys. Res.,* **98,** 6755–6804.

Banda, E., 1988. Crustal parameters in the Iberian peninsula, *Phys. Earth planet. Int.,* **51,** 222–225.

Beavan, J. & Haines, J., 2001. Contemporary horizontal velocity and strain-rate fields of the Pacific–Australian plate boundary zone through New Zealand, *J. geophys. Res.,* **106,** 741–770.

Bijwaard, H., Spakman, W. & Engdahl, E.R., 1998. Closing the gap between regional and global travel time tomography, *J. geophys. Res.,* **103,** 30 055–30 078.

Billen, M.I. & Houseman, G.A., 2004. Lithospheric instability in obliquely convergent margins: San Gabriel Mountains, Southern California, *J. geophys. Res.,* **109 (B01404),** doi:10.1029/2003JB002605.

Bird, P., 1978. Initiation of intracontinental subduction in the Himalaya, *J. geophys. Res.,* **83,** 4975–4987.

Bird, P., 1979. Continental delamination and the Colorado Plateau, *J. geophys. Res.,* **84,** 7561–7571.

Blanco, M.J. & Spakman, W., 1993. The P-wave velocity structure of the mantle below the Iberian peninsula: evidence for subducted lithosphere below southern Spain, *Tectonophysics,* **221,** 13–34.

Bullen, M.E., Burbank, D.W., Garver, J.I. & Abdrakhmatov, K.Ye., 2001. Late Cenozoic tectonic evolution of the northwestern Tien Shan: new age estimates for the initiation of mountain building, *Geol. Soc. Am. Bull.,* **113,** 1544–1559.

Burov, E.B. & Molnar, P., 1998. Gravity anomalies over the Ferghana Valley (central Asia) and intracontinental deformation, *J. geophys. Res.,* **103,** 18 137–18 152.

Calvert, A. *et al.,* 2000. Geodynamic evolution of the lithosphere and upper mantle beneath the Alboran region of the western Mediterranean: constraints from travel time tomography, *J. geophys. Res.,* **105,** 10 871–10 898.

Canright, D. & Morris, S., 1993. Buoyant instability of a viscous film over a passive fluid, *J. Fluid Mech.,* **255,** 340–372.

Chandrasekhar, S., 1961. *Hydrodynamic and Hydromagnetic Stability,* p. 652, Oxford University Press, Oxford.

Conrad, C.P., 2000. Convective instability of thickening mantle lithosphere, *Geophys. J. Int.,* **143,** 52–70.

Conrad, C.P. & Molnar, P., 1997. The growth of Rayleigh–Taylor-type instabilities in the lithosphere for various rheological and density structures, *Geophys. J. Int.,* **129,** 95–112.

Conrad, C.P. & Molnar, P., 1999. Convective instability of a boundary layer with temperature- and strain-rate-dependent viscosity in terms of 'available buoyancy,' *Geophys. J. Int.,* **139,** 51–68.

Davey, F.J. *et al.,* 1998. Preliminary results from a geophysical study across a modern, continent-continent collisional plate boundary—the Southern Alps, New Zealand, *Tectonophysics,* **288,** 221–235.

Doublas, M. & Oyarzun, R., 1989. Neogene extensional collapse in the western Mediterranean (Betic-Rif Alpine orogenic belt): implications for the genesis of the Gibraltar arc and magmatic activity, *Geology,* **17,** 430–433.

England, P.C. & Houseman, G.A., 1989. Extension during continental convergence with application to the Tibetan Plateau, *J. geophys. Res.,* **94,** 17 561–17 579.

England, P. & Molnar, P., 1997. Active deformation of Asia: from kinematics to dynamics, *Science,* **278,** 647–650.

England, P.C. & Thompson, A.B., 1984. Pressure–temperature–time paths of regional metamorphism I: Heat transfer during the evolution of regions of thickened continental crust, *J. Petrol.,* **25,** 894–928.

Griffin, W.L., O'Reilly, S.Y., Ryan, C.G., Gaul, O. & Ionov, D.A., 1998. Secular variation in the composition of subcontinental lithospheric mantle: geophysical and geodynamic implications, in *Structure and Evolution of the Australian Continent,* American Geophysical Union Geodynamics Series 26, pp. 1–26, eds Braun, J., Dooley, J., Goleby, B., van der Hilst, R. & Klootwijk, C., American Geophysical Union, Washington, DC.

Gutscher, M.-A., Malod, J., Rehault, J.-P., Contrucci, I., Klingelhoefer, F., Mendes-Victor, L. & Spakman, W., 2002. Evidences for active subduction beneath Gibraltar, *Geology,* **30,** 1071–1074.

Hatzfeld, D. & Ben Sari, D., 1977. Grands profils sismiques dans la region de l'arc de Gibraltar, *Bull. Soc. Géol. Fr.,* **7,** 749–756.

Hatzfeld, D. & Frogneux, M., 1981. Evidence of intermediate depth earthquakes around the Gibraltar area, *Nature,* **292,** 443–445.

Hirth, G. & Kohlstedt, D.L., 1996. Water in the oceanic upper mantle: implications for rheology, melt extraction and the evolution of the lithosphere, *Earth planet. Sci. Lett.,* **144,** 93–108.

Houseman, G.A. & Molnar, P., Gravitational (Rayleigh–Taylor) instability of a layer with non-linear viscosity and convective thinning of continental lithosphere, *Geophys. J. Int.,* **128,** 125–150.

Houseman, G. & Molnar, P., 2001. Mechanisms of lithospheric renewal associated with continental orogeny, in *Continental Reworking and Reactivation,* Geological Society of London Special Publication 184, pp. 13–37, eds Miller, J.A., Holdsworth, R.E., Buick, I.S. & Hand, M., Geological Society of London, London.

Houseman, G.A., McKenzie, D.P. & Molnar, P., 1981. Convective instability of a thickened boundary layer and its relevance for the thermal evolution of continental convergent belts, *J. geophys. Res.,* **86,** 6115–6132.

Houseman, G., Neil, E.A. & Kohler, M.D., 2000. Lithospheric instability beneath the Transverse Ranges of California, *J. Geophys. Res.,* **105,** 16 237–16 250.

Humphreys, E.D. & Clayton, R.W., 1990. Tomographic image of the southern California mantle, *J. geophys. Res.,* **95,** 19 725–19 746.

Humphreys, E., Clayton, R.W. & Hager, B.H., 1984. A tomographic image of mantle structure beneath southern California, *Geophys. Res. Lett.,* **11,** 625–627.

Jaupart, C., Mareschal, J.C., Guillou-Frottier, L. & Davaille, A., 1998. Heat flow and thickness of the lithosphere in the Canadian Shield, *J. geophys. Res.,* **103,** 15 269–15 286.

Jordan, T.H., 1981. Continents as a chemical boundary layer, *Phil. Trans. R. Soc. Lond.,* A, **301,** 359–373.

Kaminski, E. & Jaupart, C., 2000. Lithosphere structure beneath the Phanerozoic intracratonic basins of North America, *Earth planet Sci. Lett.,* **178,** 139–149.

Kay, R.W. & Mahlburg Kay, S., 1993. Delamination and delamination magmatism, *Tectonophysics,* **219,** 177–189.

Kohler, M.D., 1999. Lithospheric deformation beneath the San Gabriel Mountains in the southern California Transverse Ranges, *J. geophys. Res.,* **104,** 15 025–15 041.

Kohler, M.D. & Eberhart-Phillips, D., 2002. Three-dimensional lithospheric structure below the New Zealand Southern Alps, *J. geophys. Res.,* **107**(B10), 2225, doi:10.1029/2001JB000182.

Mattauer, M., 1986. Intracontinental subduction, crust-mantle décollement and crustal-stacking wedge in the Himalayas and other collision belts, in *Collision Tectonics,* Geological Society of London Special Publication 19, pp. 37–50, eds Coward, M.P. & Ries, A.C., Geological Society of London, London.

McKenna, L.W. & Walker, J.D., 1990. Geochemistry of crustally derived leucocratic igneous rocks from the Ulugh Muztagh area, northern Tibet, and their implications for the formation of the Tibetan Plateau, *J. geophys. Res.,* **95,** 21 483–21 502.

Miyashiro, A., 1973. *Metamorphism and Metamorphic Belts,* pp. 96–99, George Allen and Unwin, London.

Molnar, P., Houseman, G.A. & Conrad, C.P., 1998. Rayleigh–Taylor instability and convective thinning of mechanically thickened lithosphere: effects of non-linear viscosity decreasing exponentially with depth and of horizontal shortening of the layer, *Geophys. J. Int.,* **133,** 568–584.

Mooney, W.D. & Weaver, C.S., 1989. Regional crustal structure and tectonics of the Pacific coastal states: California, Oregon, and Washington, in *Geophysical Framework of the Continental United States,* Geological Society of America Memoir 172, pp. 129–161, eds Pakiser, L.C. & Mooney, W.D., Geological Society of America, Boulder, CO.

Mooney, W.D., Laski, G. & Masters, T.G., 1998. CRUST 5.1: a global crustal model at 5° × 5°, *J. geophys. Res.,* **103,** 727–747.

Neil, E.A. & Houseman, G.A., 1999. Rayleigh–Taylor instability of the upper mantle and its role in intraplate orogeny, *Geophys. J. Int.,* **138,** 89–107.

Oreshin, S., Vinnik, L., Peregoudov, D. & Roecker, S., 2002. Lithosphere and asthenosphere of the Tien Shan imaged by S receiver functions, *Geophys. Res. Lett.,* **29**(8), doi:10.1029/2001GL014441.

Pearce, J.A. *et al.,* 1990. Genesis of collision volcanism in eastern Turkey, *J. Volcanol. Geotherm. Res.,* **44,** 189–229.

Platt, J.P. & Vissers, R.L.M., 1989. Extensional collapse of thickened continental lithosphere: a working hypothesis for the Alboran Sea and Gibraltar Arc, *Geology,* **17,** 540–543.

Platt, J.P., Soto, J.I., Comas, M.C. & Leg 161 Shipboard Scientists, 1996. Decompression and high-temperature–low-pressure metamorphism in the exhumed floor of an extensional basin, Alboran Sea. western Mediterranean, *Geology,* **24,** 447–450.

Platt, J.P., Soto, J.-I., Whitehouse, M.J., Hurford, A.J. & Kelley, S.P., 1998. Thermal evolution, rate of exhumation, and tectonic significance of metamorphic rocks from the floor of the Alboran extensional basin, western Mediterranean, *Tectonics,* **17,** 671–689.

Plomerovà, J., Payo, G. & Babushka, V., 1993. Teleseismic P-residual study in the Iberian peninsula, *Tectonophysics,* **221,** 1–12.

Raikes, S.A., 1980. Regional variations in upper mantle structure beneath Southern California, *Geophys. J. R. astr. Soc.,* **63,** 187–216.

Reigber, Ch. *et al.,* 2001. New space geodetic constraints on the distribution of deformation in Central Asia, *Earth planet. Sci. Lett.,* **191,** 157–165.

Roecker, S.W., Sabitova, T.M., Vinnik, L.P., Burmakov, Y.A., Golvanov, M.I., Mamatkanova, R. & Munirova, L., 1993. Three-dimensional elastic wave velocity structure of the western and central Tien Shan, *J. geophys. Res.,* **98,** 15 779–15 795.

Royden, L.H., 1993. The tectonic expression of slab pull at continental convergent boundaries, *Tectonics,* **12,** 303–325.

Sclater, J.G. & Francheteau, J., 1970. The implications of terrestrial heat flow observations on current tectonic and geochemical models of crust and upper mantle of the earth, *Geophys. J. R. astr. Soc.,* **20,** 509–537.

Sclater, J.G., Parsons, B. & Jaupart, C., 1981. Oceans and continents: similarities and differences in the mechanisms of heat loss, *J. Geophys. Res.,* **86,** 11 535–11 552.

Seber, D., Barazangi, M., Ibenbrahim, A. & Demnati, A., 1996a. Geophysical evidence for lithospheric delamination beneath the Alboran Sea and Rif-Betic mountains, *Nature,* **379,** 785–790.

Seber, D., Barazangi, M., Tadili, B.A., Ramdani, M., Ibenbrahim, A. & Ben Sari, D., 1996b. Three-dimensional upper mantle structure beneath the intraplate Atlas and interplate Rif mountains of Morocco, *J. geophys. Res.,* **101,** 3125–3138.

Sengör, A.M.C. & Kidd, W.S.F., 1979. Post-collisional tectonics of the Turkish-Iranian Plateau and a comparison with Tibet, *Tectonophysics,* **55,** 361–376.

Shen, Zh.-K., Jackson, D.D. & Ge, B.X., 1996. Crustal deformation across and beyond the Los Angeles basin, from geodetic measurements, *J. geophys. Res.,* **101,** 27 957–27 980.

Sobel, E.R. & Arnaud, N., 2000. Cretaceous–Paleogene basaltic rocks of the Tuyon basin, NW China and the Kyrgyz Tian Shan: the trace of a small plume, *Lithos,* **50,** 191–215.

Soto, J.-L. & Platt, J.P., 1998. Petrological and structural evolution of high-grade metamorphic rocks from the floor of the Alboran sea Basin, western Mediterranean, *J. Petrol.,* **40,** 21–60.

Spakman, W., van der Lee, S. & van der Hilst, R., 1993. Tomographic images of the upper mantle below central European-Mediterranean mantle down to 1400 km, *Phys. Earth Planet. Int.,* **79,** 3–74.

Stern, T., Molnar, P., Okaya, D. & Eberhart-Philips, D., 2000. Teleseismic P wave delays and modes of shortening the mantle lithosphere beneath South Island, New Zealand, *J. geophys. Res.,* **105,** 21 615–21 632.

Tapponnier, P., 1977. Evolution tectonique du système alpin en Méditerrannée: Poinçonnement et écrasement rigide-plastique, *Bull. Soc. géol. France,* **XIX,** 437–460.

Tapponnier, P., Peltzer, G. & Armijo, R., 1986. On the mechanics of the collision between India and Asia, in *Collision Tectonics,* pp. 115–157, eds Coward, M.P. & Ries, A.C., Geological Society of London, London.

Tapponnier, P., Xu Zhiqin, Roger, F., Meyer, B., Arnaud, N., Wittlinger, G. & Yang Jingsui, 2001. Oblique stepwise rise and growth of the Tibet Plateau, *Science,* **294,** 1671–1677.

Turner, S., Hawkesworth, C., Liu, J., Rogers, N., Kelley, S. & van Calsteren, P., 1993. Timing of Tibetan uplift constrained by analysis of volcanic rocks, *Nature,* **364,** 50–54.

Turner, S. *et al.,* 1996. Post-collision, shoshonitic volcanism on the Tibetan Plateau: implications for convective thinning of the lithosphere and the source of ocean island basalts, *J. Petrol.,* **37,** 45–71.

Turner, S.P., Platt, J.P., George, R.M.M., Kelley, S.P., Pearson, D.G. & Nowell, G. M., 1999. Magmatism associated with orogenic collapse of the Betic-Alboran domain, SE Spain, *J. Petrol.,* **40,** 1011–1036.

Vinnik, L.P. & Saipbekova, A.M., 1984. Structure of the lithosphere and asthenosphere of the Tien Shan, *Ann. Geophys.,* **2,** 621–626.

Wellman, H.W., 1979. An uplift map for the south island of New Zealand and a model for uplift of the Southern Alps, in *The Origin of the Southern Alps,* Bulletin of the Royal Society of New Zealand no 18, pp. 13–20, eds Walcott, R.I. & Cresswell, M.M., Royal. Society of New Zealand, Wellington.

Willett, S.D. & Beaumont, C., 1994. Subduction of Asian lithospheric mantle beneath Tibet inferred from models of continental collision, *Nature,* **369,** 642–645.

Working Group for Deep Seismic Sounding in the Alboran Sea 1974, 1978. Crustal seismic profiles in the Alboran Sea—Preliminary results, *Pure Appl. Geophys.,* **116,** 167–180.